DIFFUSION BARRIERS/ADHESION PROMOTERS. SURFACE AND INTERFACIAL STUDIES OF COPPER AND COPPER-ALUMINUM ALLOYS

Krupanand Solomon Shepherd, B.S., M.S.

Dissertation Prepared for the Degree of

DOCTOR OF PHILOSOPHY

UNIVERSITY OF NORTH TEXAS

August 2000

APPROVED:

Jeffry A. Kelber, Major Professor
William E. Acree, Jr., Committee Member
Paul S. Braterman, Committee Member
David E. Golden, Committee Member
Ruthanne D. Thomas, Chair of the Department of Chemistry
C. Neal Tate, Dean of the Robert B. Toulouse School of Graduate Studies

Shepherd, Krupanand Solomon, Diffusion barriers/adhesion promoters. Surface and interfacial studies of copper and copper-aluminum alloys. Doctor of Philosophy (Chemistry), August 2000, 81 pp., 4 tables, 41 illustrations, references, 80 titles.

The focus of this research is to study the interaction between copper and the diffusion barrier/adhesion promoter. The behavior of copper sputter-deposited onto sputter-cleaned tantalum nitride is investigated. The data show that copper growth on tantalum nitride proceeds with the formation of 3-D islands, indicating poor adhesion characteristics between copper and $Ta_{0.4}N$. Post-annealing experiments indicate that copper will diffuse into $Ta_{0.4}N$ at 800 K. Although the data suggests that $Ta_{0.4}N$ is effective in preventing copper diffusion, copper's inability to wet $Ta_{0.4}N$ will render this barrier ineffective.

The interaction of copper with oxidized tantalum silicon nitride (O/TaSiN) is characterized. The data indicate that initial copper depositions result in the formation a conformal ionic layer followed by Cu(0) formation in subsequent depositions. Post-deposition annealing experiments performed indicate that although diffusion does not occur for temperatures less than 800 K, copper "de-wetting" occurs for temperatures above 500 K. These results indicate that in conditions where the substrate has been oxidized facile de-wetting of copper may occur.

The behavior of a sputter-deposited $Cu_{0.6}Al_{0.4}$ film with SiO_2 ($Cu_{0.6}Al_{0.4}/SiO_2$) is investigated. The data indicate that aluminum segregates to the SiO_2 interface and

ACKNOWLEDGMENTS

The author wishes to express his sincere appreciation to Professor Jeff Kelber for the guidance and careful instruction he has provided. The author would also like to acknowledge the Semiconductor Research Corporation and Motorola Inc. for financial funding of this research. Finally, the author would like to thank his family for their encouragement.

TABLE OF CONTENTS

LIST OF TABLES

LIST OF ILLUSTRATIONS

CHAPTER 1

INTRODUCTION

As demand has grown for semiconductor products with higher performance and lower power, the level of integration has increased. The increase in the level of integration has primarily been accomplished by scaling down the physical size of the transistor. The continued scaling of the transistor has resulted in a disparity between device and interconnect technology. Although the signal propagates through the transistor faster as the transistor is scaled down, signal propagation through the interconnect network has become slower [1]. As a result, high demands have been placed on interconnect technology. These demands have placed heavy strains on aluminum technology and have ushered in the copper era.

Copper is considered the primary candidate to replace Al as the interconnect due to its superior resistance to electromigration and its lower resistivity [2]. However, the use of Cu in chip metallization is not without obstacles. These obstacles include the poor adhesion of copper to SiO_2 and the rapid diffusion of copper through SiO_2 [2]. Therefore, new materials are under investigation to serve as diffusion barriers and adhesion promoters. The studies presented here focus on the surface interactions of copper with potential diffusion barriers, particularly the ability of copper to wet these substrates. The methodologies employed in these studies include DC magnetron sputtering and x-ray photoelectron spectroscopy (XPS). These studies include:

(1) The nucleation behavior, thermal stability (dewetting), and diffusion behavior of copper on an oxidized TaSiN substrate and

(2) The nucleation behavior, thermal stability (dewetting), and diffusion behavior of $Cu_{0.6}Al_{0.4}$ films at the SiO_2 interface.

This dissertation consists of three chapters. The first chapter is devoted to a discussion of interconnect technology and experimental methodology. In chapter 2, a model study is presented that investigates the interactions of copper with an oxidized diffusion barrier. Specifically, the details of the interfacial behavior of copper with an oxidized TaSiN film are presented. Chapter 3 investigates the interaction of copper-aluminum alloys at the SiO_2 interface. Copper-aluminum alloys have been proposed as self-developing barriers for ultra large scale integration (ULSI) and gigascale integration (GSI) manufacturing [2].

1.1. Interconnect Delays

As scaling of the device dimensions continues, signal propagation through the transistor has become faster, while signal propagation through the interconnects has become slower. For example, as the channel length of the metal oxide field effect transistor (MOSFET) decreases, the carrier transit time across the channel also decreases. However, these signals must propagate through the interconnect network which are the basic charge carriers. It is clear that for feature sizes < 0.50 μm, the interconnect delay will dominate the intrinsic gate delay (Figure 1.1) [1].

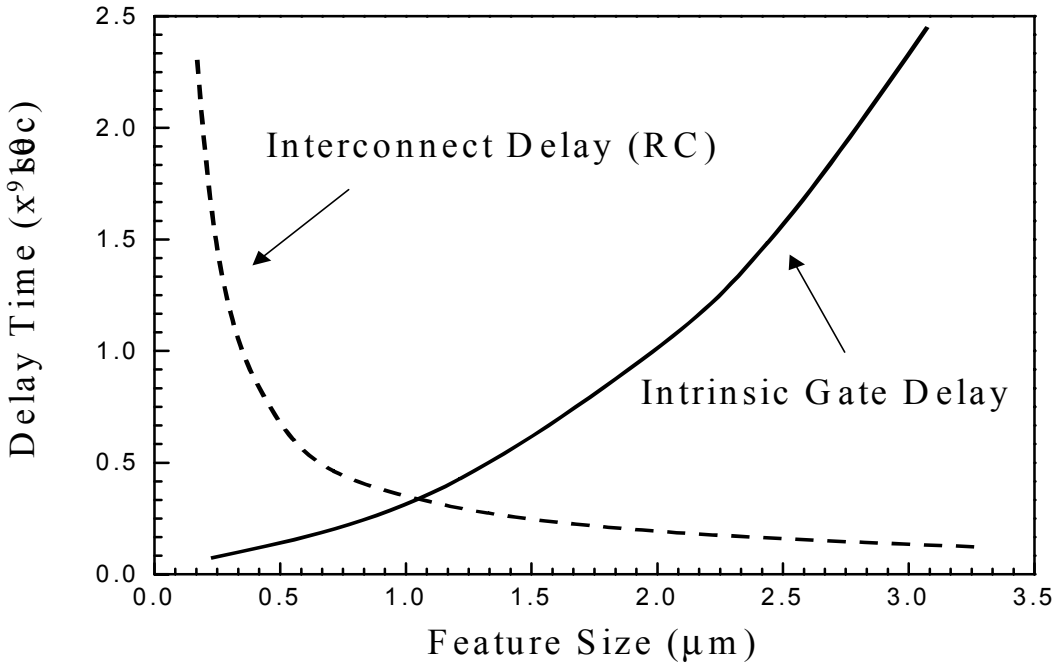

Figure 1.1. Comparison of intrinsic gate delay and interconnect (RC) delay as a function of the feature size.[1]

The interconnect delay can be approximated by the *RC* delay, where *R* is the effective total resistance of the interconnection and *C* is the capacitance associated with the dielectric.

$$RC \approx \rho \varepsilon \frac{L^2}{t_M t_{ILD}} \qquad (1\text{-}1)$$

In Eq. (1-1), ρ, L, and t_M refer to the resistivity, length, and thickness of the interconnect respectively, while ε and t_{ILD} refer to the permittivity and the thickness of the interlevel dielectric. The permittivity, ε, is usually expressed in terms of the dielectric constant κ, defined as $\varepsilon/\varepsilon_o$ where ε_o is the permittivity of space.

By considering the expression for *RC* delay presented in Eq. (1-1), the simplest method to reduce the *RC* delay in a multilevel interconnection network (MLI), shown in Figure 1.2, is to use a lower resistivity metal isolated by lower dielectric constant materials.

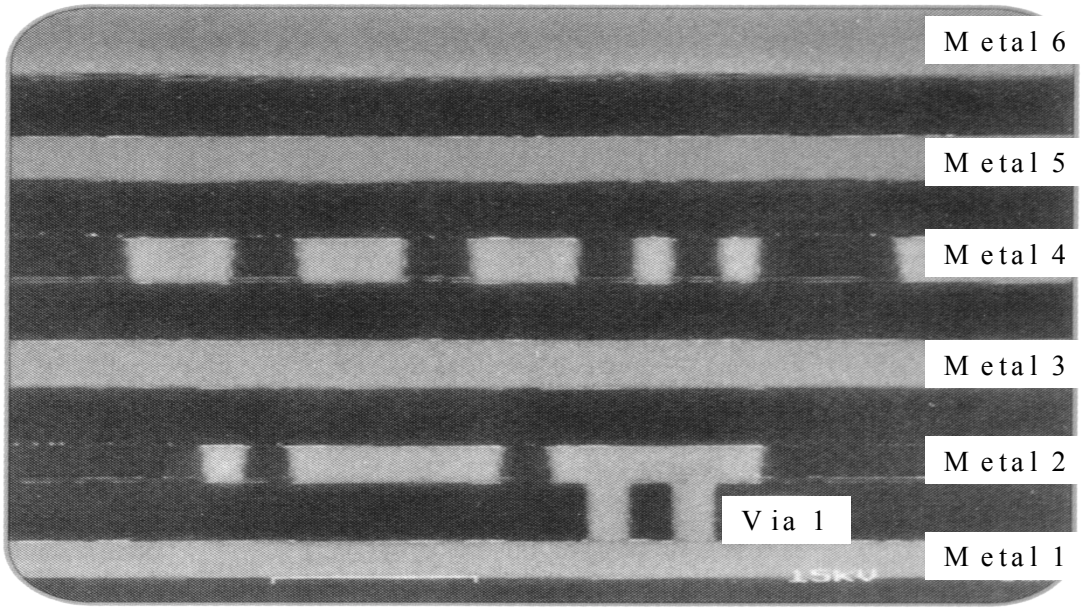

Figure 1.2. The cross section of MLI (6 levels) with copper interconnects and SiO_2 insulators.[3]

1.2. Interconnect Metal Alternatives

Aluminum has been used extensively by the semiconductor industry for interconnect applications. Aluminum's low resistivity and its ability to reduce SiO_2, leading to a very stable interface Al/SiO_2 interface, has led to Al's successful integration in VLSI manufacturing [2,4]. Despite these favorable characteristics, Al's poor resistance to electromigration and its low melting point makes the replacement of Al in ULSI and

GSI manufacturing inevitable. Interconnect metals that have been considered as replacements for Al include Cu, Ag, and Au [2,5,6].

The properties of Cu, Ag, Au are contrasted with that of Al in Table 1.1. All of these metals have a lower resistivity than aluminum, with Ag being the least resistive. When considering Au, it is clear from Table 1.1 that Au is inferior to copper in every respect except for its excellent resistance to corrosion. The only real contender other than copper then is silver. Silver posses a slight edge over copper in terms of resistivity (5 %), but loses any edge it may have possessed when considering electromigration.

From the discussions above, it is clear that Cu is the best choice to replace Al. However, there are several issues that must be addressed before Cu can be fully integrated with device manufacturing. These issues include the rapid drift of Cu through SiO_2 under thermal stress and/or applied electrical fields and copper's inability to adhere to SiO_2 [7-9]. Therefore, diffusion barriers (materials that can block the transport of Cu) and adhesion promoters (materials that improve the interfacial stability between Cu and the dielectric) must be found before Cu can be fully integrated into device manufacturing.

1.3. Adhesion Promoters and Diffusion Barriers

The interaction between two materials can be either chemical or physical (van der Waals forces). Interactions that are purely disperse and relatively weak cannot withstand the mechanical or thermal stress that is encountered under typical processing conditions. Therefore, a good adhesion promoter must react chemically with the substrate. The chemical reaction that a good adhesion promoter must have with its

Table 1.1. Possible Interconnect Materials Properties

Property		Metal			
		Al	Cu	Ag	Au
Resistivity (μΩ-cm)		2.66	1.67	1.59	2.35
Melting Point (°C)		660	1085	962	1064
Electromigration Resistance		Low	Very High	Low	High
Corrosion in Air		Low	High	High	Very Low
Adhesion to SiO_2		Good	Poor	Poor	Poor
Deposition	Sputtering	Yes	Yes	Yes	Yes
	Evaporation	Yes	Yes	Yes	Yes
	CVD	Yes	Yes	?	?
Etching	Dry	Yes	Yes	Yes	Yes
	Wet	Yes	Yes	Yes	Yes

substrate is very specific. The reaction that must occur at the interface between the adhesion promoter and the substrate must be self-limiting. Reactions that are not self-limiting may proceed so far into the substrate that the integrity of the substrate is

compromised. The interface that occurs when an Al layer interacts with a SiO_2 is self-limiting at low process temperatures [2,4].

$$3SiO_2 + 4Al \longrightarrow 2Al_2O_3 + 3Si \qquad (1\text{-}2)$$

or

$$xSiO_2 + yAl \longrightarrow Al_ySi_xO_{2x} + (x-z)Si \qquad (1\text{-}3)$$

Unlike the Al/SiO_2 system, the adhesion between Cu and SiO_2 is weak [7,10]. Cu is also known to readily diffuse through SiO_2 under either thermal or electrical stressing,[7-9,11] which can lead to the formation of deep traps in the underlying Si substrate [12,13]. For these reasons, many efforts are being expended to design an effective diffusion barrier/adhesion promoter for copper. Attempts to resolve these problems have led to the use a thin metal layer that acts as a 'glue' layer between the dielectric and the copper. Materials that have been considered for the 'glue' layer include Ti, Ta, and Cu-Al and Cu-Mg alloys. All these materials have demonstrated the ability to adhere to the dielectric [2,14-16].

In selecting potential diffusion barriers, the mutual diffusivity of the materials (Cu and diffusion barrier) and the metallurgical stability of the Cu/diffusion barrier interaction must be considered [2,6,17]. Since the diffusivity is related to the melting point of the host material, the best diffusion barriers usually have the highest melting points (e.g. refractory metals/metal compounds) [6]. In addition, refractory metals such as Ta, W, Mo, and V are not expected to be miscible with Cu at low temperature, *i.e. they have a low reactivity towards copper* [17]. A high solid solubility of Cu in the barrier metal can lead to the formation of metal-Cu binary phases which could compromise the integrity of

the barrier if the reaction is not self-limiting [2]. Finally, barriers can fail based on structural considerations.

Diffusion barrier metals have traditionally been polycrystalline in nature. The usage of polycrystalline materials over their single crystal analogs has stemmed from the high cost considerations of the later. In the case of polycrystalline metals, barrier integrity can be compromised via grain boundary diffusion [18,19]. This phenomenon is largely responsible for failures in conventional metallization [20]. Efforts to inhibit diffusion in these polycrystalline materials has included stuffing the grain boundaries with impurities such as O, N, and C and, more recently, the adoption of amorphous diffusion barriers [18,20,21]. By incorporating amorphous diffusion barriers with high crystallization temperatures, such as TaSiN, into the metallization scheme, it is possible to entirely circumvent the grain boundary diffusion [20,22].

1.4. Thin Film Growth Process

There are three general categories of growth modes in the thin film process (Figure 1.3). In the Volmer-Weber (VM) or island formation mode, growth occurs with the formation of 3-dimensional small clusters directly on the substrate, which then grow into larger clusters that coalesce. Growth occurs in this way because in the VW mode the atoms or molecules of the deposited material are more strongly bound to the each other than to the substrate. The layer-by-layer or Frank-van der Merwe (FM) mode exhibits the opposite behavior; the adsorbate-substrate interactions are stronger than

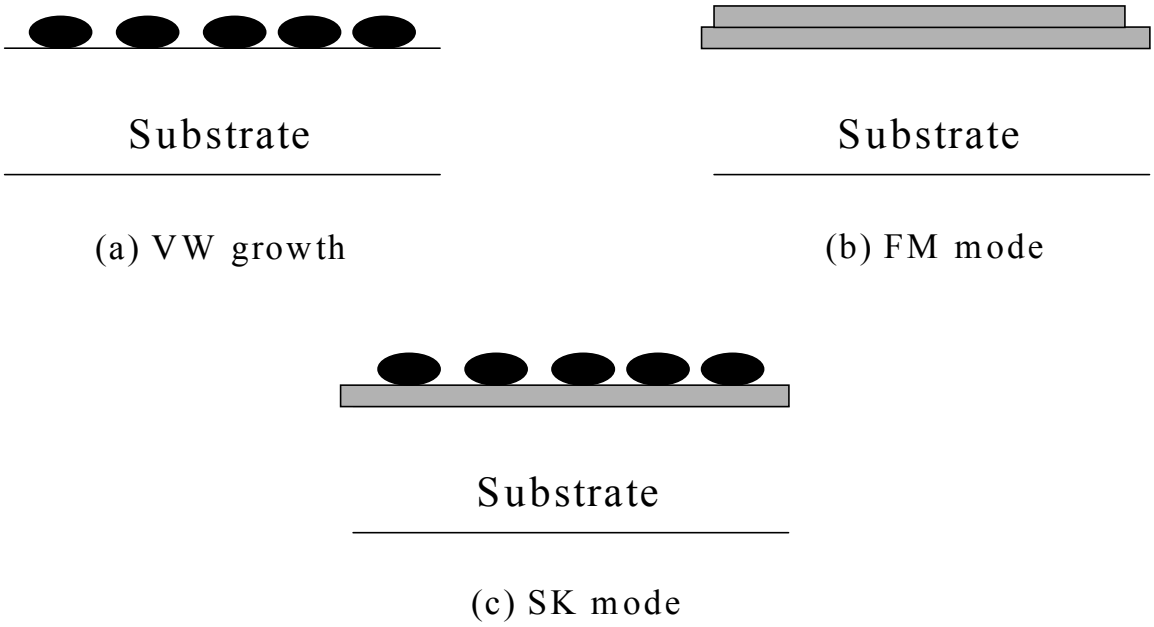

Figure 1.3. Three Modes of Film Growth.

adsorbate-adsorbate interactions in the FM mode. FM growth occurs when there is a monotonic decrease in binding energy toward the bulk crystal value of the deposit [23]. The third mode of growth, Stranski-Krastanov (SK) mode, occurs with conformal growth in the first layer or several layers followed by islanding in the subsequent layers. This can occur when there is a disruption in the monotonic decrease in binding energy, which is characteristic of FM growth [23]. In both FM and SK modes, conformal growth or 'wetting' occurs in the first layer. The wetting behavior for a film can be expressed using the following expression: [24]

$$\Delta\gamma = \gamma_F + \gamma_{FS} - \gamma_S \qquad (1\text{-}4)$$

where γ_F, γ_S, and γ_{FS} are the surface free energies of the film, the substrate and the film-substrate interface, respectively. Wetting will occur for $\Delta\gamma < 0$.[24] In the metal/metal oxide system, γ_{FS} must be large and negative for wetting to occur, since, $\gamma_{metals} > \gamma_{oxides}$.[24]

1.5. Combined XPS and DC Magnetron Sputtering Apparatus

The XPS/DC magnetron sputtering system is used to study the ability of copper to 'wet' various substrates. This approach combines XPS acquisition and sputter deposition without intermediate sample exposure to the atmosphere. This methodology enables a careful characterization of metal-substrate interface as a function of deposition. These kinds of studies are of interest when determining the adhesion or 'wetting' of a film to its substrate.

1.5.1. Apparatus.

The combined XPS and DC magnetron sputtering apparatus used in this research is shown in schematically in Figure 1.4. The main chamber is equipped with a dual anode ray source, an ion-sputtering gun and a hemispherical analyzer equipped for XPS. The design of the sputter chamber is such that it can be isolated from the analysis chamber. In addition, the target has been position approximately 11" away from the substrate so that deposition rates on the order of 0.1 Å/min can be achieved.

1.5.2. Methodology

The design of the combined XPS and DC magnetron sputtering chamber (Figure 1.4) allows monitoring of the film substrate interface as a function of coverage using XPS. The experiment begins with analysis of the substrate prior to deposition. Following this analysis, material is sputter deposited onto the substrate and examined by XPS. This

cycle of deposition and XPS analysis is repeated many times so that enough data is generated so that an uptake curve can be derived. An uptake curve is the intensity of the deposited overlayer plotted against some estimate of coverage of the overlayer. Using this uptake curve, important information can be ascertained concerning the morphology of the deposited film.

The wetting behavior of a deposited film on a substrate can be determined from an uptake curve. For the experiments performed in the following chapters, the XPS signal

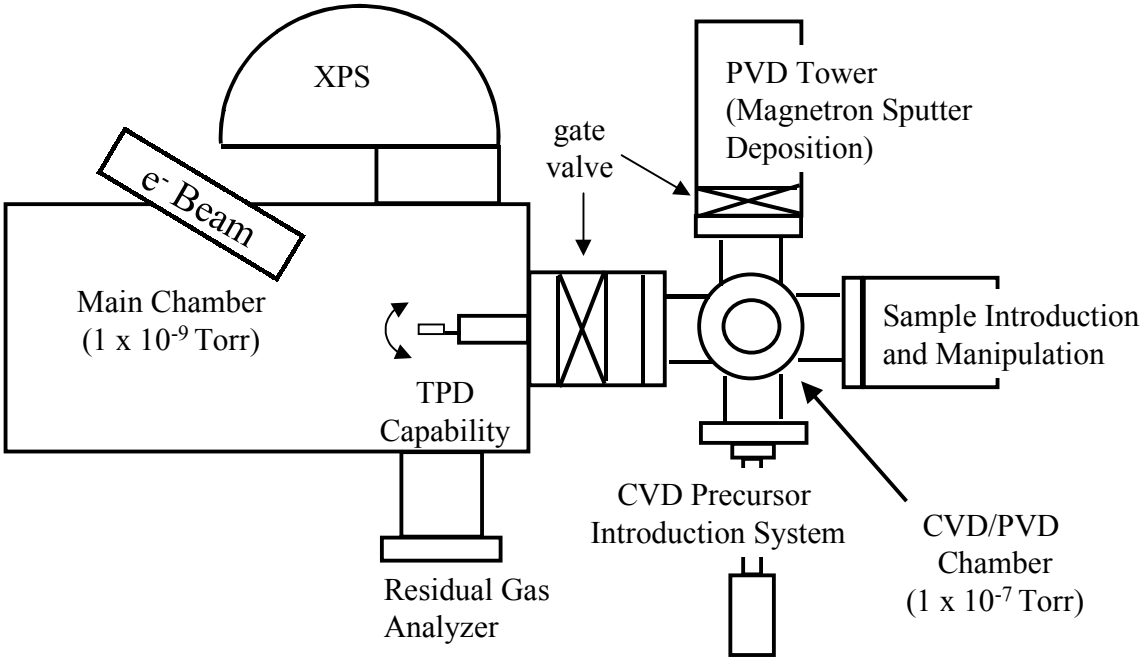

Figure 1.4. Combined XPS and DC Magnetron Sputtering Apparatus

of the deposited overlayer used in the uptake curves has been normalized with respect to the XPS signal from the substrate. This normalization method takes account of changes in X-ray flux to the sample that can arise from sample transfer back and forth from the XPS

analysis chamber to the deposition chamber during the course of an experiment. In cases of conformal growth (Figure 1.5a), a change in slope in the uptake curve is expected. That is, the normalized intensity of the deposited overlayer has a linear relationship to the surface coverage of the copper in the first ad-layer. Similarly, the normalized intensity of the deposited overlayer has a linear relationship to the surface coverage in the second layer and subsequent layers, but with different slopes due to the attenuation of the intensity of the previous layer by subsequent layers [25,26]. For VW growth or poor

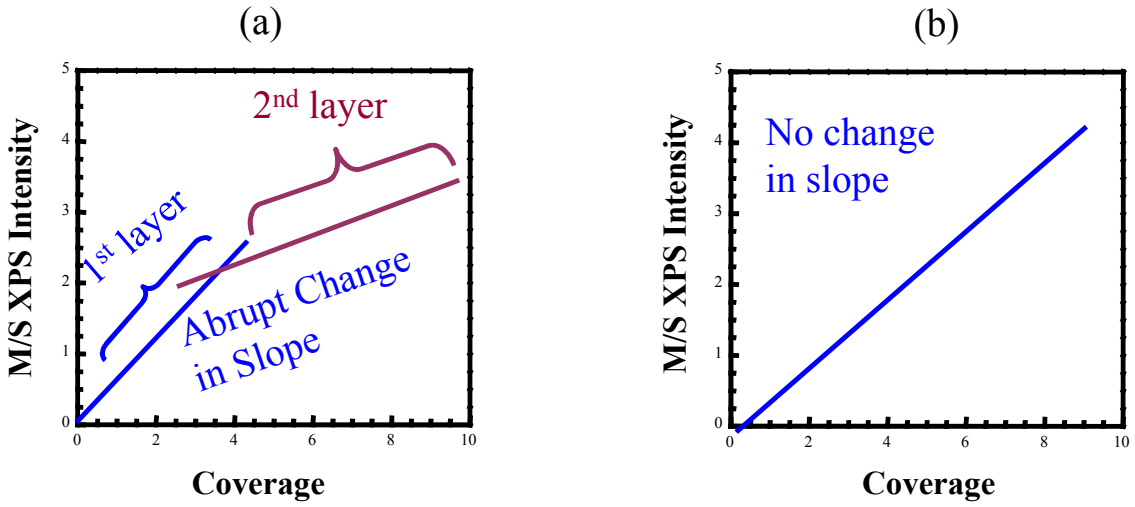

Figure 1.5. Uptake Curves for (a) conformal growth or wetting and (b) poor wetting.

wetting (Figure 1.5b), the uptake curves will exhibit near linear or continuous behavior till coalescence sets in, since layer-by-layer attenuation does not occur [25,27,28].

1.5.3. X-ray Photoelectron Spectroscopy

X-ray photoelectron spectroscopy (XPS), also termed electron spectroscopy for chemical analysis (ESCA), was developed by Kai Siegbahn and his fellow researchers in the 1950s. In 1966, Seigbhan published results that indicated that XPS is a surface sensitive technique [29]. The surface sensitivity of XPS combined with its ability to ascertain both qualitative and quantitative chemical information has made XPS one of the most broadly used surface analysis techniques used today. In addition to these advantages, XPS is the least invasive of all the electron and ion spectroscopy techniques, having the ability to detect all elements except hydrogen and helium [30].

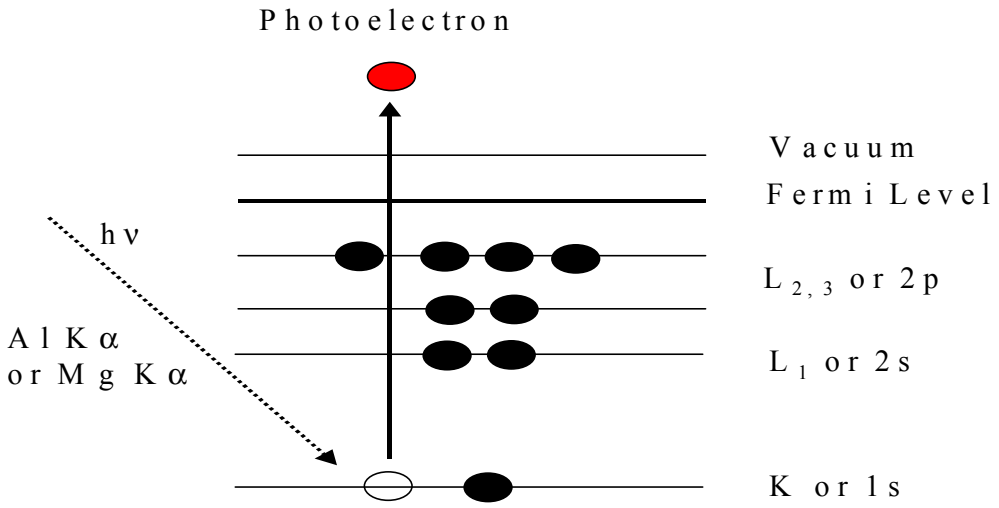

Figure 1.6. Schematic of XPS emission process for a model atom.

Surface analysis using XPS occurs by interaction of an X-ray photon with a sample, which leads to the ejection of photoelectrons (Fig. 1.6). Typically, the soft X-ray sources are either Mg or Al anodes. These anodes are used for their relatively narrow

linewidths and high photon energies [31]. A photon of sufficiently high energy, Mg Kα (1253.6 eV) or Al Kα (1486.6 eV) can ionize an atom producing a photoelectron. The kinetic energy of the photoelectron is governed by

$$KE = h\nu - BE - \phi_s \qquad (1\text{-}5)$$

where hν is the kinetic energy of the photon, BE is the binding energy of the atomic orbital from where the electron originates, and ϕ_s is the spectrometer work function (a constant for a given analyzer). By measuring the kinetic energy of the photoelectron, the binding energy can be determined using Eq. (1-5).

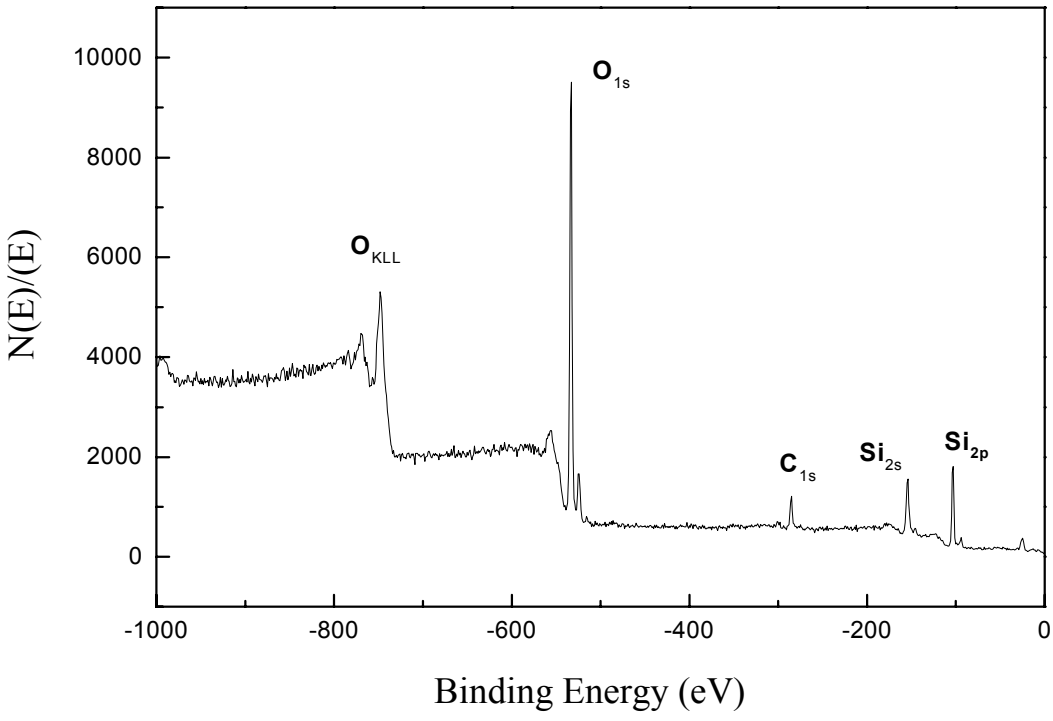

Figure 1.7. Full scan of X-ray photoelectron spectrum of SiO_2.

The binding energy of the photoelectron is an intrinsic property of the material being investigated [32]. A typical XPS spectrum is presented in Figure 1.7. The spectrum is obtained by plotting the number of detected electrons versus the binding energy. Each element has a unique set of binding energies that can shift depending on its chemical environment. Shifts in the binding energy of an element arise from differences in the chemical potential and the polarizability of the compounds [30]. Therefore, XPS can be used to map changes in the oxidation state and other chemical details. In addition to chemical information, quantitative information can be obtained from XPS peak areas.

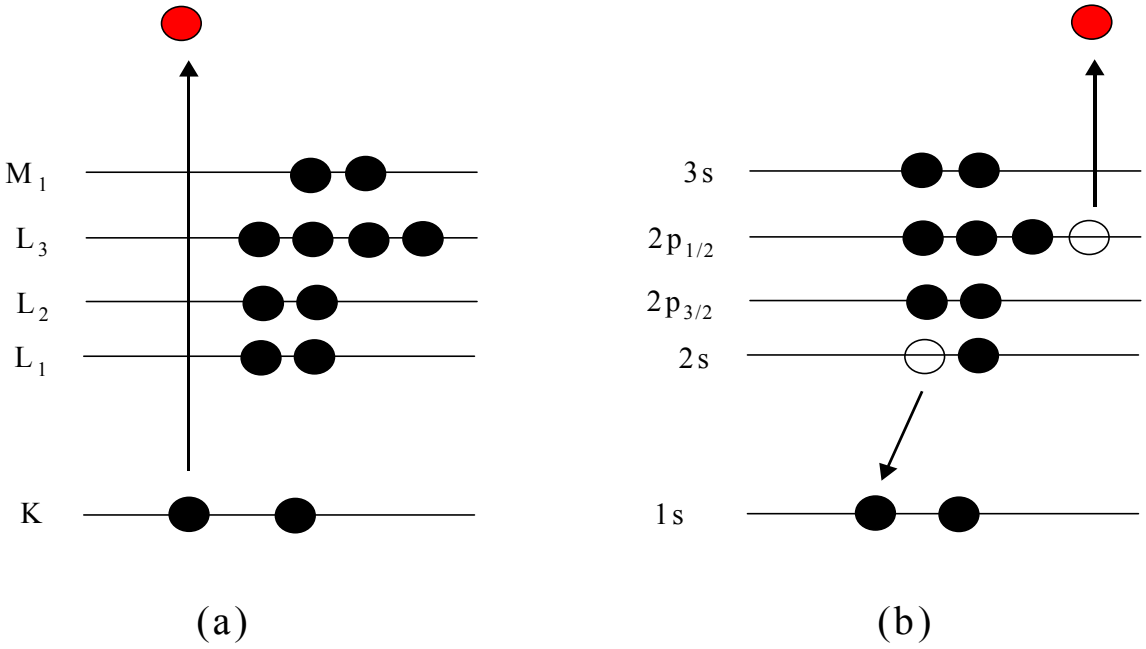

Figure 1.8. Schematic of the Auger process of a model atom. Step (a) is the initial photoelectron process and step (b) is the emission of the Auger electron.

Besides the ejection of photoelectrons, X-ray excited Auger electrons are emitted as a result of the relaxation of the excited ions remaining after the photoemission process.

The Auger process (Figure 1.8) involves three energy levels: an empty core level (K-shell) and two higher levels (L or M shells). For an X-ray excited Auger process, the initial empty core level (the electron vacancy with energy E_K) is created with an X-ray. The core level is then filled with an outer electron (with energy, E_{L1}) and with the excess energy (E_{L3}) being emitted simultaneously in the form of a second electron, the Auger electron. In contrast to the photoelectron in XPS, the energy of the Auger electron is

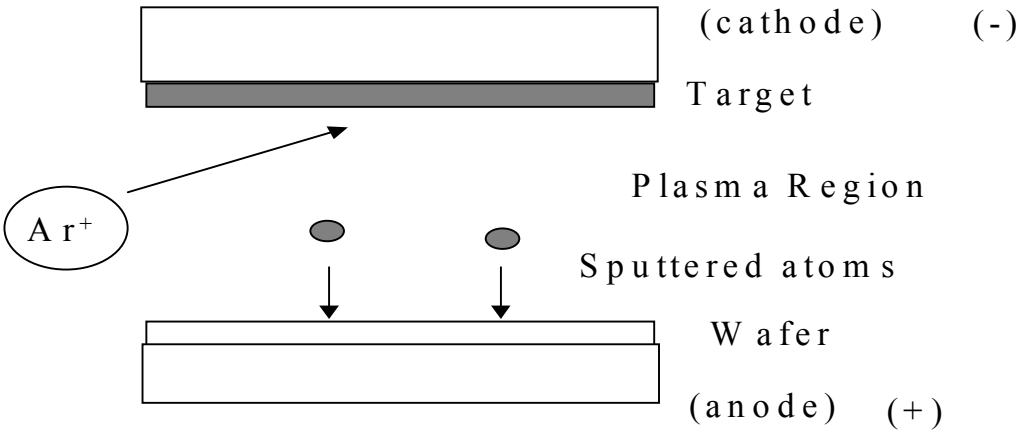

Figure 1.9. The DC diode sputtering process.

independent of the excitation source and is primarily due to the difference between the energy of the initial ion and the doubly charged final ion. For the KLL transition (Figure 1.8), the energy of the Auger electron is given by:

$$E_A = E_K - E_{L1} - E_{L3} \qquad (1\text{-}6)$$

where K = 1s, L_1 and L_2 refer to the 2s and $2p_{1/2}$ shells, respectively. The energy of the Auger electron is characteristic of the element in the sample and in special cases can be used to extract chemical bonding information from Auger peak energy positions and lineshapes.

1.5.4. DC Magnetron Sputtering

Sputtering is the act of bombardment of a surface with energetic particles such as accelerated ions. In the process surface atoms of the solid are scattered backward due to the collisions between the surface atoms and the energetic particles. The term sputtering is also synonymous with cathode sputtering.

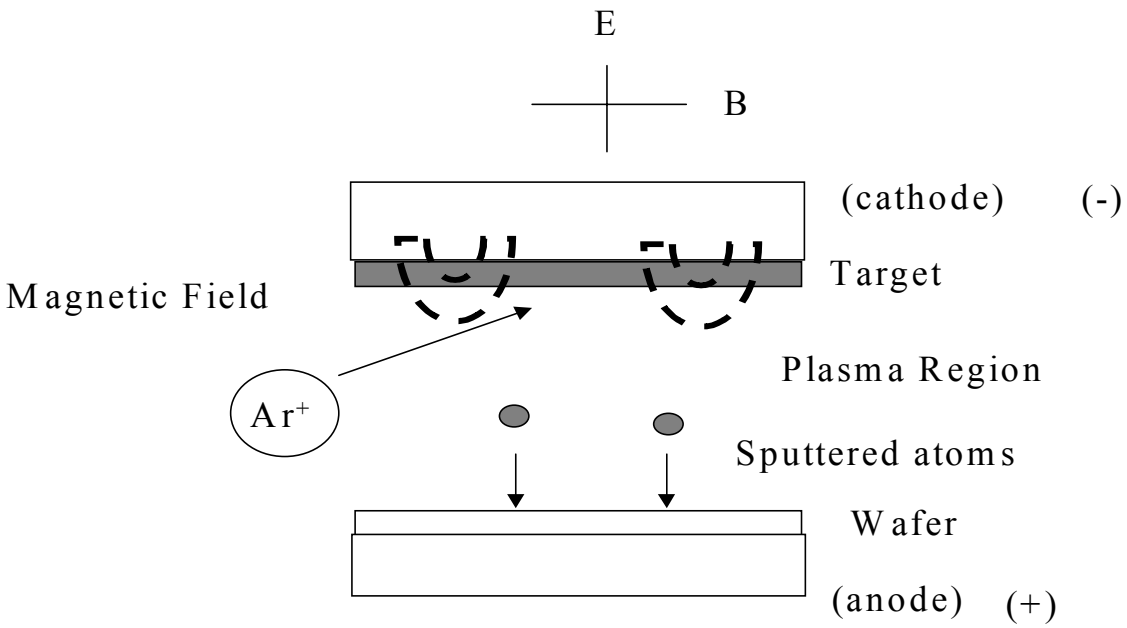

Figure 1.10. The DC magnetron sputtering process.

The simplest sputtering system is dc diode sputtering. The dc sputtering system (Figure 1.9) is composed of a pair of planar electrodes. In this system, the front of the cathode is covered with the material to be sputtered, while the substrate sits on the anode. The sputtering gas pressure in the sputtering chamber is typically 0.1 Torr [33]. The glow discharge created by the application of a dc voltage between the electrodes, results in

acceleration of the Ar^+ ions toward the target and the deposition of thin films on the substrate.

In dc magnetron sputtering (Figure 1.10), a magnetic field is imposed on the cathode and glow discharge, which is parallel to the cathode surface. In this way, the magnetic field is oriented in such a way that the electrons are forced to move in a closed loop. This electron trapping results in a greater ionization efficiency of the Ar atoms. This improved ionization efficiency has resulted in a technique that allows higher sputtering rates at lower pressures and less gas incorporation into these sputtered films [33]. The operating pressures for DC magnetron sputtering can be performed at pressures as low as 10^{-4} Torr [33].

1.6. Chapter References

[1] Jeng, S.-P.; Havemann, R. H.; Chang, M. C. *Process Integration and Manufacturability Issues for High Performance Multilevel Interconnect*; Jeng, S.-P.; Havemann, R. H.; Chang, M. C., Ed.; MRS: San Francisco, CA, 1994; Vol. 337, pp 25.

[2] Murarka, S. P. *Materials and Science Engineering* **1997**, *R19*, 85-151.

[3] Singer, P. *Semiconductor International* **1999**, *13*, 67-70.

[4] Strausser, Y. E.; Scheibner, E. J.; Johannssen, J. S. *Thin Solid Films* **1978**, *52*, 203-214.

[5] Murarka, S. P. *Metallization Theory and Practice for VLSI and ULSI*; Murarka, S. P., Ed.; Butterworth: New York, New York, 1992, pp Chap. 1.

[6] Murarka, S. P.; Hymes, S. W. *Crit. Rev. In Sol. St. and Mat. Sci.* **1995**, *20*, 87-124.

[7] Zhou, J. B.; Gustafsson, T.; Garfunkel, E. *Surface Science* **1997**, *372*, 21-27.

[8] Raghavan, G.; Chiang, C.; Anders, P. B.; Tzeng, S.-M.; Villasol, R.; Bai, G.; Bohr, M.; Fraser, D. B. *Thin Solid Films* **1995**, *262*, 168-176.

[9] Loke, A. L. S.; Ryu, C.; Yue, C. P.; Cho, J. S. H.; Wong, S. S. *IEE Electron Device Letters* **1996**, *17*, 549-551.

[10] Zhou, J. B.; Lu, H. C.; Gustaffson, T. *Surface Science Letters* **1993**, *293*, L887-L892.

[11] Mcbrayer, J. D.; Swanson, R. M.; Sigmon, T. W. *J. Electrochem. Soc.* **1986**, *123*, 1242.

[12] Broniatowski, A. *Phys. Rev. Lett.* **1989**, *62*, 3074.

[13] Gupta, D. *Mater. Chem. Phys.* **1995**, *41*, 199-205.

[14] Pretorius, R.; Harris, J. M.; Nicolet, M.-A. *Solid-State Electron* **1978**, *21*, 667.

[15] De Filipe, T. S.; Murarka, S. P.; Bedell, S.; Lanford, W. A. *Thin Solid Films* **1998**, *335*, 49-53.

[16] Ding, P. J.; Lanford, W. A.; Hymes, S.; Murarka, S. P. *J. Appl. Phys.* **1994**, *75*, 3627-3631.

[17] Li, J.; Shacham-Diamand, Y.; Mayer, J. W. *Mater. Sci. Rep.* **1992**, *9*, 1-51.

[18] Nicolet, M.-A.; Bartur, M. *JVST* **1981**, *19*, 786-793.

[19] Nicolet, M.-A. *Thin Solid Films* **1978**, *52*, 415-443.

[20] Nicolet, M.-A.; Suni, I.; Finetti, M. *Solid State Technol.* **1983**, *26*, 129.

[21] Dalal, H. M.; Ghafghaichi, M.; Kasprazak, L. A.; Wimpfheimer, H. ; Dalal, H. M.; Ghafghaichi, M.; Kasprazak, L. A.; Wimpfheimer, H., Ed.: U.S., 1980; Vol. 4 206 472.

[22] Wiley, J. D.; Perepezko, J. H.; Nordman, J. E.; Guo, K.-J. *IEEE Transactions on Industrial Electronics* **1982**, *IE-29*, 154-157.

[23] Venables, J. A.; Spiller, G. D. T.; Hanbucken, M. *Rep. Prog. Phys.* **1984**, *47*, 399.

[24] Zhang, L.; Persaud, R.; Madey, T. E. *Physical Review B* **1997**, *56*, 549-556.

[25] Shepherd, K.; Kelber, J. A. *Applied Surface Science* **1999**, *151*, 287-298.

[26] Kelber, J. A.; Niu, C.; Shepherd, K. *Surface Science* **2000**, *446*, 76-88.

[27] Feldman, L. C.; Mayer, J. W. *Fundamentals of Surface and Thin Film Analysis*; Feldman, L. C.; Mayer, J. W., Ed.; P T R Prentice-Hall, Inc.: EngleWood Cliffs, New Jersey, 1986, pp 352.

[28] Wu, M.-C.; Goodman, D. W. *J. Phys. Chem.* **1994**, *98*, 9874-9881.

[29] Larsson, K.; Nordling, C.; Siegbahn, K. *Acta. Chem. Scand.* **1966**, *20*, 2880.

[30] Moulder, J. F.; Stickle, W. F.; Sobol, P. E.; Bomben, K. D. *Handbook of X-ray Photoelectron Spectroscopy*; Moulder, J. F.; Stickle, W. F.; Sobol, P. E.; Bomben, K. D., Ed.; Physical Electronics, Inc.: Eden Prarie, Minnesota, 1992.

[31] Seah, M. P. *Practical Surface Analysis*; 2nd ed.; Seah, M. P., Ed.; John Wiley & Sons: New York, 1990; Vol. 1, pp 51.

[32] Watts, J. F. *Vacuum* **1994**, *45*, 653-671.

[33] Wasa, K.; Hayakawa, S. *Handbook of Sputter Deposition Technology, Principles Technology and Applications*; Wasa, K.; Hayakawa, S., Ed.; Noyes Publications: Park Ridge, New Jersey, 1992, pp 304.

CHAPTER 2

INTERACTIONS OF COPPER ON SPUTTER-CLEANED TANTALUM NITRIDE

2.1. Introduction.

The transition of interconnect materials, from aluminum to copper, has led to a concerted efforts to investigate tantalum and tantalum-based materials as diffusion barrier candidates. Studies regarding tantalum's effectiveness as a diffusion barrier indicate that Cu will diffuse into tantalum anywhere from 310 °C to 630 °C [1]. The exact diffusion temperature is dependent on the microstructure of the film and the deposition conditions under which the film is deposited [1]. In the case of tantalum, the microstructure is typically polycrystalline and consists of grain boundaries that can act as fast diffusion pathways [2]. For this reason, impurities (C, N, O) are often used to stuff grain boundaries [3-5].

In the case of tantalum doped with nitrogen, the diffusion temperature of Cu into the substrate is significantly raised for barriers of equivalent thickness [6]. Unfortunately, a high diffusion temperature alone does not constitute the only criterion for being an effective diffusion barrier. In addition to having a high diffusion temperature, Cu must be able to adhere or wet the substrate. In this regard, few accounts can be found in the literature regarding the wetting behavior of copper on tantalum

nitride. In this study, we report the wetting and diffusion behavior of copper on tantalum nitride.

2.2. Experimental Methodologies

XPS and sputter deposition experiments were performed in a UHV system shown schematically in Section 1.5. The ultra high vacuum system (UHV) consisted of a main chamber and a sputter deposition chamber. X-ray photoelectron spectra were acquired in the main chamber with a base pressure of 1 x 10^{-9} Torr. Spectra were obtained using an unmonochromatized MgKα x-ray source (PHI model 1427) operated at 15 keV and 300 Watts and a hemispherical analyzer (VG100AX) operated in the constant pass energy mode (50 eV). Collected data were referenced to an energy scale calibrated with binding energies of Au($4f_{7/2}$) at 84.0 eV and Cu($2p_{3/2}$) at 932.7 eV [7]. Grazing incidence spectra were obtained by rotating the sample 60° off surface normal. XPS data analysis was carried out using commercially available software (ESCA Tools) which utilizes Gaussian-Lorentzian functions to synthesize peak components [8]. Shirley background subtraction, proven to be very effective in fitting the short energy range found in typical core level XPS spectral synthesis, was adopted in this study [9,10]. Atomic concentrations were calculated with atomic sensitivity factors specific for the hemispherical analyzer(VG100AX) and were obtained directly from the manufacturer. Relative concentrations were determined using the following equation:

$$N_x = \frac{I_x}{S_x} \Big/ \sum_i \frac{I_i}{S_i} \qquad (2\text{-}2)$$

where N is the number of atoms of the element x per unit volume, I is the intensity of photoelectron signal detected per second, and S is the atomic sensitivity factor appropriate to the analyzer[7,11].

DC magnetron sputtering was performed in the sputter deposition chamber with a base pressure of 1 x 10^{-7} Torr. Sputter deposition was accomplished using a planar magnetron sputtering source (Mini Mak) operated in constant power mode of 150 Watts and an operating pressure of 15 millitorr of Argon. Argon of 99.999% purity and a copper target of 99.999% purity were used for sputter deposition.

The sample, obtained from Motorola Inc., consisted of a 1 cm^2 500 Å thick tantalum nitride film on a 1000 Å thick SiO_2 film grown on a Si(100) wafer. The sample was rinsed with ethanol and placed into the UHV analysis chamber. X-ray photoelectron spectra of the sample were then acquired to determine the chemical composition of the air-exposed sample surface. The sample was then subject to N_2 sputter cleaning followed by further XPS analysis. Next, the sample was introduced to the deposition chamber where magnetron sputtering of copper onto the sample is performed. Target to substrate distances were such that deposition rates of ~ 0.1 Å/min were achievable, allowing a study of the film/substrate interface. Temperatures were monitored by a chromel-alumel thermocouple spot-welded between a thin titanium foil and the sample.

2.3. Results

2.3.1. Characterization of tantalum nitride

The percent composition for tantalum nitride including contamination effects is provided in Table 2.1. The compositions were calculated using equation 2-2. The data

Table 2.1. Atomic Composition of Sputter-Cleaned $Ta_{0.4}N$.

	Surface Normal, %	Grazing Incidence, %
Ta	25.9	20.4
N	62.9	69.3
O	11.2	9.6

indicate the Ta:N ratio is 0.4. The data also indicate that the sample is vertically homogeneous, since the composition does not vary appreciably with the analysis depth. X-ray photoelectron (XP) spectra of the sputter-cleaned tantalum nitride are shown in Figures 2.1a-2.3b. The figures include spectra that were acquired with the sample of the surface at 90° (surface normal) and 30° (grazing incidence) relative to the analyzer. Examination of the XP spectra of tantalum nitride after sputter cleaning revealed the absence of any carbon contamination, which precluded internal referencing of the spectra to adventitious carbon. Therefore, all spectra in this study are referenced to the $Ta(4f_{7/2})$ photoelectron line of $Ta_{0.4}N$, which has a binding energy of 23.2 eV [12]. The $Ta(4f_{7/2})$ binding energy of $Ta_{0.4}N$ is higher than the reported values for TaN (22.6 eV).[12] Higher binding energies can be expected for the $Ta(4f_{7/2})$ photoelectron line as the nitrogen composition increases [12]. Examination of the Ta(4f) data (Figures 2.1a & 2.1b) indicate the presence of several chemical environments. The Ta(4f) spectra include both the $Ta(4f_{7/2})$ and the $Ta(4f_{5/2})$ photoelectron lines. These doublets are well fit with a FWHM of 1.8 eV. Fitting of the spectra was accomplished using a gaussian-lorentzian doublet

with a 4:3 intensity for the Ta($4f_{7/2}$) and the Ta($4f_{5/2}$), respectively and a 1.9 eV separation [7]. The binding energies that are reported here refer to the binding energy of

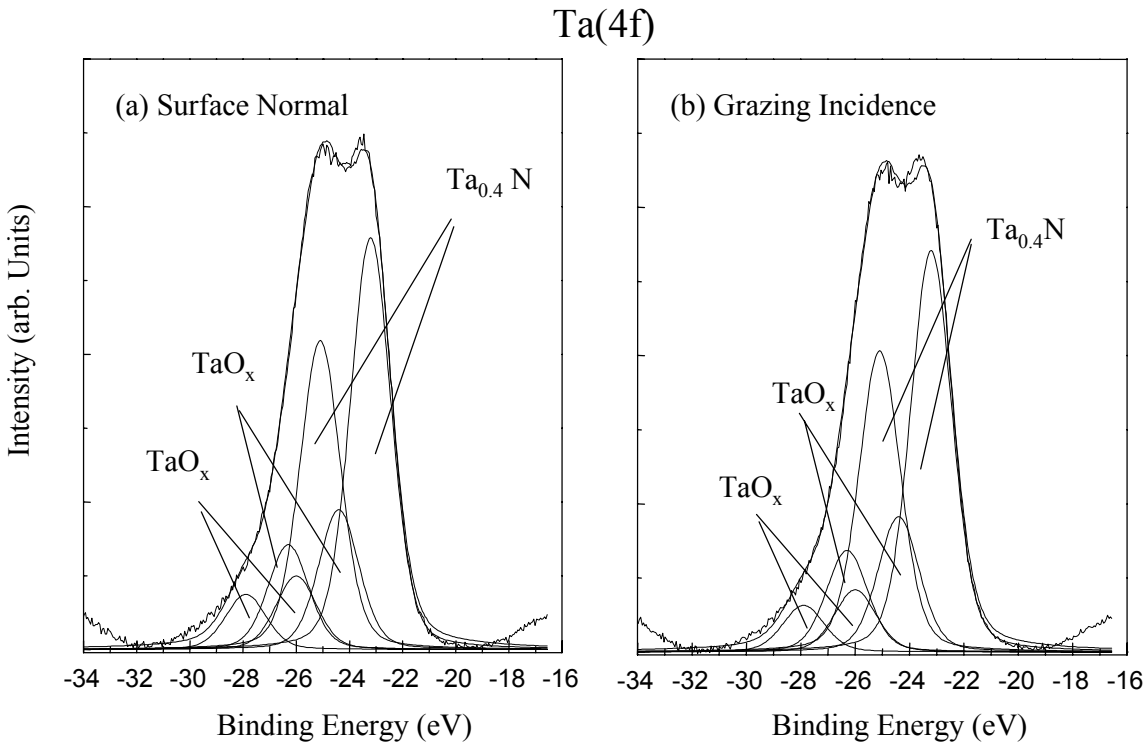

Figure 2.1. XPS Ta(4f) spectra of $Ta_{0.4}N$. (a) Surface Normal. (b) Grazing Incidence.

the Ta($4f_{7/2}$) photoelectron line. The doublet at 23.2 eV agrees well with literature values for $Ta_{0.4}N$ [12], while the doublets at 24.4 eV and 26.0 eV fall in the range of tantalum suboxides [13]. The N(1s) spectra shown in Figure 2.2a & 2.2b overlap with the Ta($4p_{3/2}$) photoelectron lines. This region is well fit using a FWHM of 2.7 eV for the N(1s) photoelectron line and a FWHM of 3.7 eV for the Ta($4p_{3/2}$) photoelectron line. The binding energy of the N(1s) photoelectron line is 397.1 eV which is in the range of

reported values for other nitrides [7]. The Ta($4p_{3/2}$) spectra indicate the presence of three environments and correlate with the fit of the Ta(4f) spectra (Figure 2.1). The Ta($4p_{3/2}$)

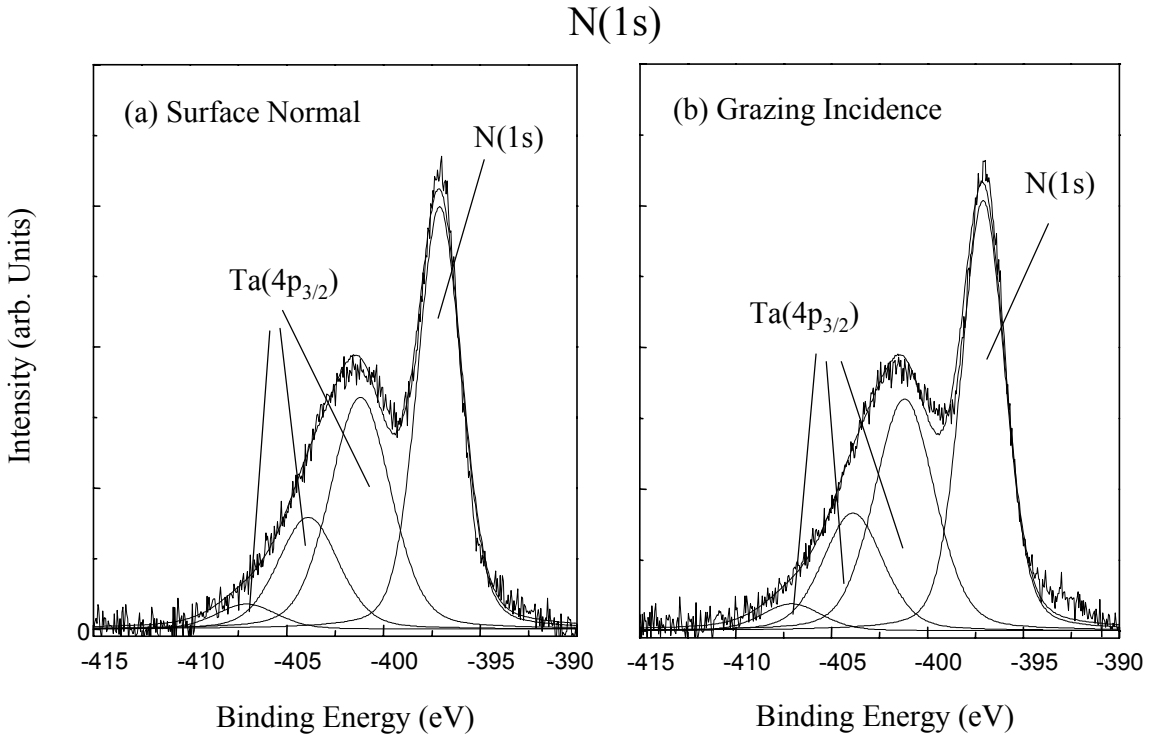

Figure 2.2. XPS N(1s) spectra of $Ta_{0.4}N$. (a) Surface Normal. (b) Grazing Incidence.

photoelectron line at 401.2 eV is assigned to $Ta_{0.4}N$, while the peak positions at 403.9 eV and 407.1 eV are assigned to tantalum suboxides. Examination of the O(1s) spectra (Figure 2.3) indicate the presence of two enrironments. These environments are fit with a FWHM of 2.1 eV [14]. Their binding energies are 529.9 eV and 531.3 eV and correspond with the two suboxides found in the Ta(4f) spectra. Their binding energies fall within the range of other metal oxides [7]. The presence of M-OH species could not be entirely ruled out since hydroxide binding energies fall in the range from 531 eV to 532 eV.

In summary, the data (Figures 2.1-2.3 and Table 2.1) combine to indicate a uniform film composition in the surface normal and grazing incidence spectra. The data

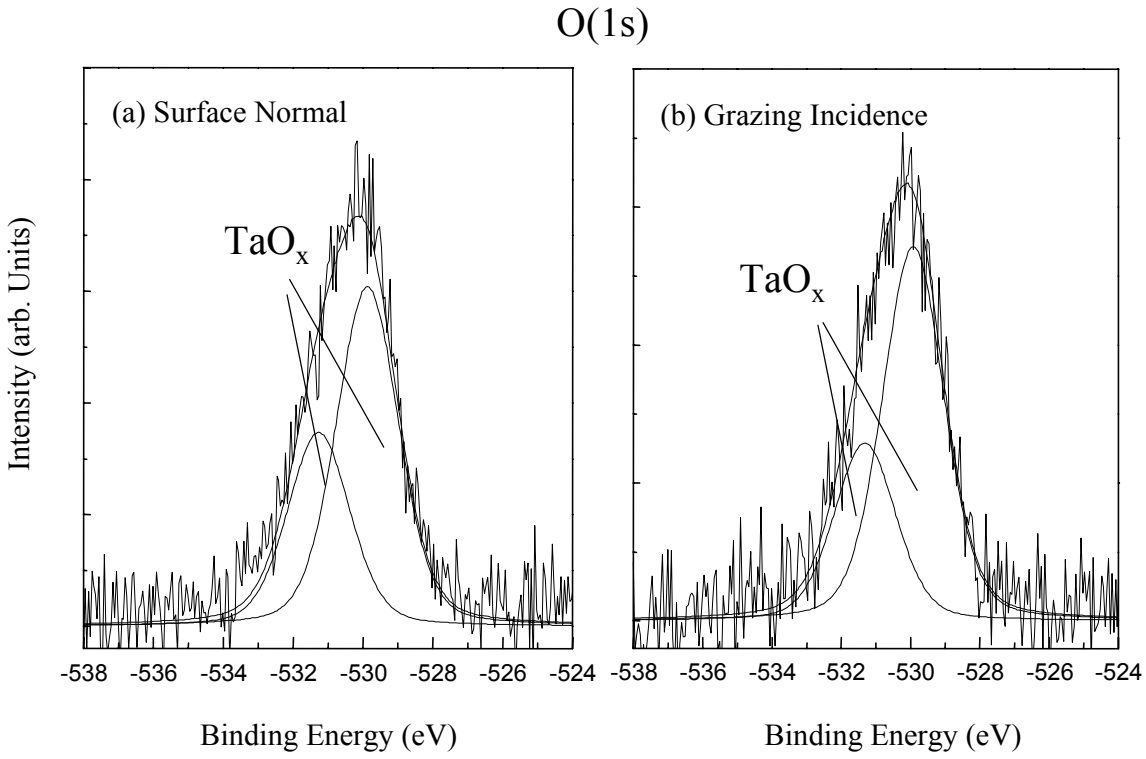

Figure 2.3. XPS O(1s) spectra of $Ta_{0.4}N$. (a) Surface Normal. (b) Grazing Incidence.

indicate the composition of the film to be primarily $Ta_{0.4}N$. The film was devoid of carbon contamination but showed some oxygen contamination. The levels of oxygen contamination were determined to be ~ 10 % resulting in the formation of TaO_x species.

2.3.2. Copper Growth on Tantalum Nitride

Copper was sputter-deposited onto the sputter-cleaned tantalum nitride surface in sequential depositions of 120 s each. Following each deposition, the XP spectra were acquired to monitor the growth of copper on tantalum nitride. The mode of growth of the

Cu overlayer can be characterized by monitoring the increase in copper XPS intensity (relative to the Ta) as a function of deposition time. The resulting uptake curve (Figure 2.4a) exhibits linear behavior. The data (Figure 2.4a) indicate that copper growth occurs with the formation of 3-D islands on sputter-cleaned tantalum nitride. In addition to the uptake curve, X-ray excited Cu(L_3VV) spectra (Figure 2.4b) were also monitored. The X-ray excited Cu(L_3VV) provides a "fingerprint" of the oxidation state of the deposited copper [15]. The feature at 917.7eV (Figure 2.4b) indicates that Cu is deposited as Cu(0) [16-18]. Using a modified Auger parameter {α = KE of Cu(L_3VV) maximum + BE of Cu($2p_{3/2}$)}, further information can be gathered from data [19]. The calculated Auger parameter is 1850.3 eV. The value is lower than the reported values for bulk Cu (1851.3 eV) [7]. The low Auger parameter can be attributed to the ineffective screening that occurs for metallic copper coverages of less than 0.5 Å average thickness [20]. In the case of small clusters, the core-hole would be poorly screened due to a low number of neighboring metal atoms.[21] The reduction in screening results in a reduction in the relaxation energy, which also result in an increase in the core-level binding energy (low Auger parameter).[21]

2.3.3. Thermal Stability of Copper on Tantalum Nitride

After 24 minutes of copper deposition, the tantalum nitride sample was annealed for 10 minutes in increments of a 100 degrees (Figure 2.5a). Annealing of the sample resulted in a decrease of the Cu/Ta XPS intensity beginning at 600 K (Figure 2.5a). In addition to the decrease in Cu/Ta XPS intensity observed at 600 K, changes were also

observed in the Auger parameter at this temperature. The Auger parameter increased from 1850.3 eV at 300 K to 1851.3 eV at 600 K. Since, the Auger parameter is not

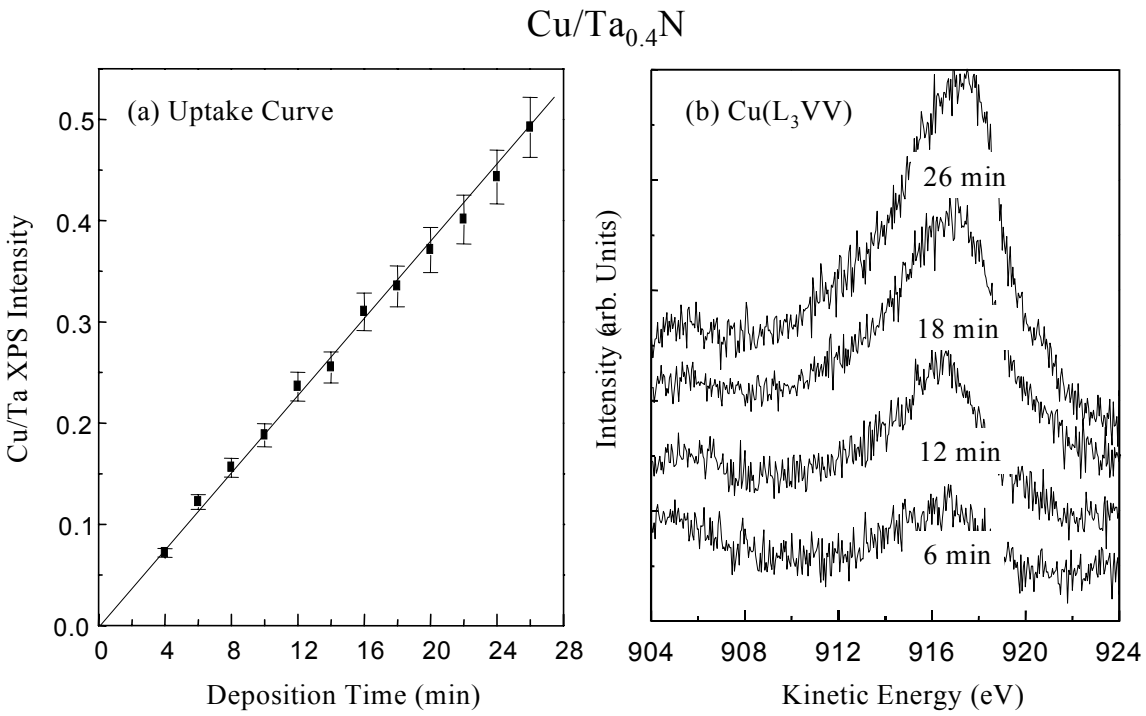

Figure 2.4. (a) $Cu/Ta_{0.4}N$ Uptake Curve. (b) $Cu(L_3VV)$ Evolution for $Cu/Ta_{0.4}N$ as a Function of Deposition Time.

reflecting a change in the oxidation state of copper, the positive shift in Auger parameter values is attributed to the change in cluster size that occurs during annealing [20]. The data indicate that while copper forms small clusters when deposited at 300 K, these clusters coalesce to form larger clusters when annealed to 600 K. Other corroborating data for this change in cluster size also includes the narrowing of the $Cu(2p_{3/2})$ photoelectron line upon annealing. The narrowing of the $Cu(2p_{3/2})$ photoelectron line from a FWHM of 2.2 eV to 2.1 eV suggests a change from varying sized copper clusters upon initial deposition at 300 K to a larger and more homogeneous cluster size after annealing to 600 K

[20,22,23]. These data also account for the observed decrease of the Cu/Ta XPS intensity ratio observed at 600 K (Figure 2.5a). The formation of larger clusters results in further

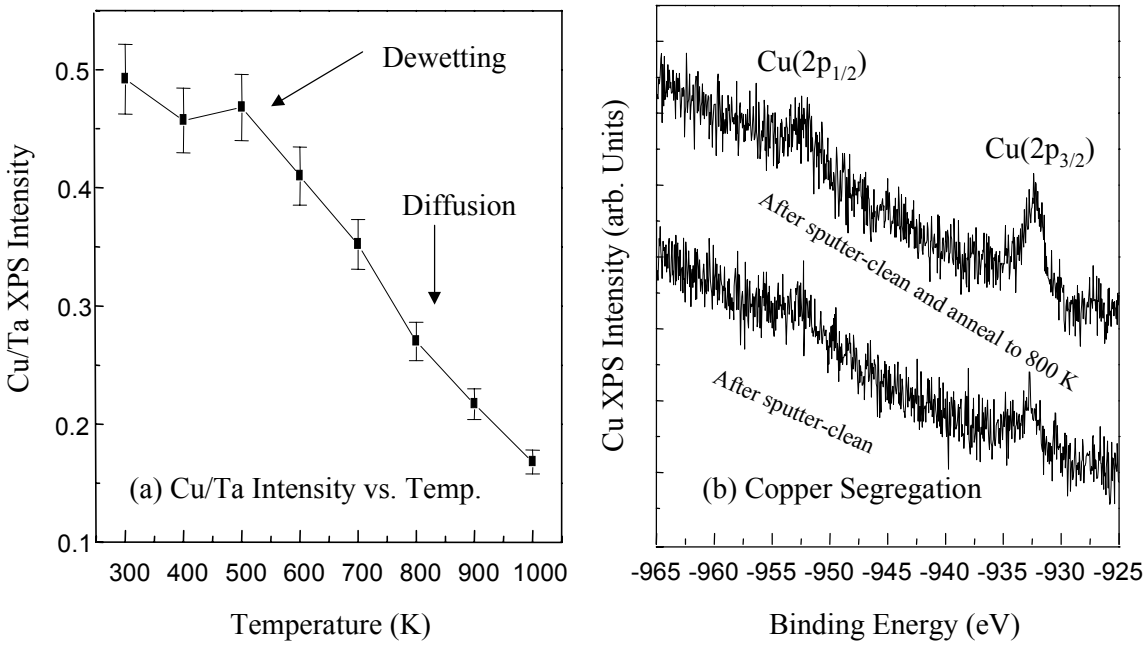

Figure 2.5. (a) Relative Cu intensity vs. annealing temperature for Cu on $Ta_{0.4}N$. (b) $Cu(2p_{3/2})$ spectral evidence of copper segregation.

attenuation of the copper signal of the copper atoms within the cluster. The formation of larger clusters, however, is only a partial explanation for what is observed in Figure 2.5a.

The continued decrease of the Cu/Ta XPS intensity (Figure 2.5a) cannot be entirely explained for the whole temperature range (600 K to 1000 K) as a result of only agglomeration. Since, the decrease in the Cu/Ta XPS intensity can also be explained by diffusion, experiments were devised to distinguish agglomeration from diffusion. Copper was sputter-deposited for 24 min onto a $Ta_{0.4}N$ sample. Next, the sample was annealed to the suspected diffusion temperature for 20 minutes. After annealing at the suspected diffusion temperature, the sample was sputter-cleaned to remove copper from the $Ta_{0.4}N$

surface. The sample was then annealed again to the suspected diffusion temperature and XP spectra acquired to determine if copper segregated from the bulk. The above experiment was performed for at the temperatures of 600 K, 700 K, 800 K, 900 K, and a 1000 K. For temperatures of 800 K and above, Cu segregation from the $Ta_{0.4}N$ sample was observed (Figure 2.5b). The data indicate that copper diffusion occurs ~ 800 K (Figures 2.5a & 2.5b).

2.4. Discussion

The data presented above (Figures 2.4a & 2.4b) demonstrate that copper initially deposited onto $Ta_{0.4}N$ at 300 K is deposited in small clusters. Upon annealing the substrate to 600 K, these clusters coalesce into larger clusters. Annealing of the substrate to 600 K resulted in an increase of the Auger parameter from 1850.3 eV to 1851.3 eV and a decrease in the FWHM. Since these changes do not reflect a change in the oxidation state from Cu(0), we infer that the smaller copper clusters coalesce to form larger clusters. For both the cases described above, the formation of clusters can be attributed to the weak interaction of the copper with substrate. In the case of $Ta_{0.4}N$, copper-copper interactions are far stronger than copper-substrate interactions.

Further annealing of $Ta_{0.4}N$ results in a continued decrease of the Cu/Ta XPS intensity (Figure 2.5a). Experiments performed indicate that copper that has diffused into $Ta_{0.4}N$ will segregate out when annealed to ~ 800 K (Figure 2.5b). The data indicate that copper will diffuse into $Ta_{0.4}N$ ~ 800 K (Figures 2.5a & 2.5b).

2.5. Conclusions

Copper is sputter-deposited onto sputter-cleaned tantalum nitride. XPS results indicate the composition of the film to be $Ta_{0.4}N$ with 10 % oxygen and no evidence of carbon contamination. The oxygen contamination results in the formation of a TaO_x species. The data also indicates the film to be vertically homogeneous with similar oxygen content in both the surface normal and grazing incidence spectra. Copper deposition onto $Ta_{0.4}N$ results in Volmer-Weber growth. Annealing of the substrate to 600 K results in further agglomeration of the clusters resulting in the formation of larger copper clusters. Copper diffusion is observed to occur at ~ 800 K. The data indicate that poor wetting of copper on $Ta_{0.4}N$ may render it an ineffective diffusion barrier.

2.6. References

[1] Clevenger, L. A.; Bojarczuk, N. A.; Hollaway, K.; Harper, J. M. E.; Carbal, C. J.; Schad, R. G.; Cardone, F.; Stolt, L. *J. Appl. Phys.* **1993**, *73*, 300-308.

[2] Jing-Cheng, L.; Lee, C. *Electrochemical and Solid-State Letters* **1999**, *2*, 181-183.

[3] Catania, P.; Doyle, J. A.; Cuomo, J. J. *JVST* **1992**, *A 10*, 3318-3321.

[4] Nicolet, M.-A.; Bartur, M. *JVST* **1981**, *19*, 786-793.

[5] Holloway, K.; Fryer, P. M.; Cyril Cabral, J.; Harper, J. M. E.; Bailey, P. J.; Keller, K. H. *J. Appl. Phys.* **1992**, *71*, 5433-5444.

[6] Stavrev, M.; Wenzel, C.; Moller, A.; Drescher, K. *Applied Surface Science* **1995**, *91*, 257-262.

[7] Moulder, J. F.; Stickle, W. F.; Sobol, P. E.; Bomben, K. D. *Handbook of X-ray Photoelectron Spectroscopy*; Moulder, J. F.; Stickle, W. F.; Sobol, P. E.; Bomben, K. D., Ed.; Physical Electronics, Inc.: Eden Prarie, Minnesota, 1992.

[8] *ESCA Tools*; 4.6 ed.; Surface/Interface Inc., Mountain View, CA., 1995.

[9] Shirley, D. A. *Phys. Rev. B* **1972**, *5*, 4709.

[10] Sherwood, P. M. A. *J. Vac. Sci. Technol. A* **1995**, *14*, 1424.

[11] Seah, M. P. *Practical Surface Analysis*; 2nd ed.; Seah, M. P., Ed.; John Wiley & Sons: New York, 1990; Vol. 1, pp 201-251.

[12] Baba, K.; Hatada, R. *Surface amd Coatings Technology* **1996**, *84*, 429-433.

[13] An, C. H.; Sugimoto, K. *J. Electrochem. Soc.* **1994**, *141*, 853-858.

[14] Shepherd, K.; Kelber, J. A. *Applied Surface Science* **1999**, *151*, 287-298.

[15] Shoen, G. *Journal of Electron Sprectroscopy and Related Phenomena* **1972**, *7*, 377.

[16] Wagner, C. D. *Discuss. Faraday Soc.* **1975**, *60*, 291.

[17] Klein, J. C.; Proctor, A.; Hercules, D. M.; Black, J. F. *Anal. Chem* **1983**, *55*, 2055.

[18] Kowalczky, S. P.; Pollak, R. A.; McFeely, F. R.; Ley, L.; Shirley, D. A. *Phys. Rev. B* **1973**, *8*, 2387.

[19] Garenstroom, S. W.; Winograd, N. *J. Chem. Phys.* **1977**, *67*, 3500.

[20] Wu, Y.; Garfunkel, E.; Madey, T. E. *J. Vac. Sci. Technol. A* **1996**, *14*, 1662-1667.

[21] Vijayakrishnan, V.; Rao, C. N. R. *Surface Science Letters* **1991**, *255*, L516-L522.

[22] Jirka, I. *Surf. Sci* **1990**, *232*, 307.

[23] W. F. Egelhoff, J. *Surf. Sci. Rep.* **1987**, *6*, 253.

CHAPTER 3

INTERACTIONS OF COPPER WITH OXIDIZED TASIN

3.1. Introduction

As microelectronic devices shrink, the replacement of aluminum by copper in interconnects is being realized. Copper is a better conductor and has a greater resistance to electromigration than aluminum [1]. Copper integration into these devices, however, has been limited by issues of copper diffusion into silicon and the consequent degradation of electronic properties. Diffusion barriers such as tantalum and tantalum-based materials are attractive candidates since they do not react with copper. Typically, these materials are polycrystalline. One disadvantage of polycrystalline materials is that grain boundary diffusion may occur at relatively low activation energies. A possible alternative is an amorphous barrier such as TaSiN, since it lacks grain boundaries that can act as diffusion pathways [2-4].

Nicolet *et al.* have investigated the diffusion properties of Cu sputter deposited onto clean TaSiN [5-7]. Clean surfaces obtained in UHV or near UHV condition are representative of substrates encountered when using cluster tools where a very high vacuum environment is constantly maintained [8]. Air exposed TaSiN is of relevance as a possible candidate in device manufacturing where substrates are exposed to air or relatively poor vacuum between processing steps [8]. In this study, we report the effects of

air exposure on the surface composition of TaSiN and its influence on the ability of copper to wet and adhere to TaSiN, as determined by XPS.

3.2. Experimental Methodologies

XPS and sputter deposition experiments were performed in a UHV system described in Section 1.5. The ultra high vacuum system (UHV) consisted of a main chamber and a sputter deposition chamber. X-ray photoelectron spectra were acquired in the main chamber with a base pressure of 1 x 10^{-9} Torr. Spectra were obtained using an unmonochromatized MgKα x-ray source (PHI model 1427) operated at 15 keV and 300 Watts and a hemispherical analyzer (VG100AX) operated in the constant pass energy mode (50 eV). Collected data were referenced to an energy scale calibrated with binding energies of Au($4f_{7/2}$) at 84.0 eV and Cu($2p_{3/2}$) at 932.7 eV [9]. The observed binding energies were affected by sample charging during acquisition. The C(1s) binding energy of adventitious carbon was set at 285.0 eV and used as a reference for the calibration of other peak positions [10]. Grazing incidence spectra were obtained by rotating the sample 60° off surface normal. XPS data analysis was carried out using commercially available software (ESCA Tools) which utilizes Gaussian-Lorentzian functions to synthesize peak components [11]. Shirley background subtraction, proven to be very effective in fitting the short energy range found in typical core level XPS spectral synthesis, was adopted in this study [12,13]. Atomic concentrations were calculated with atomic sensitivity factors specific

for the hemispherical analyzer(VG100AX) and were obtained directly from the manufacturer. Relative concentrations were determined using the following equation:

$$N_x = \frac{I_x}{S_x} \Big/ \sum_i \frac{I_i}{S_i} \qquad (3\text{-}1)$$

where N is the relative concentration of atoms of the element x per unit volume, I is the intensity of photoelectron signal detected per second, and S is the atomic sensitivity factor appropriate to the analyzer [9, 14].

DC magnetron sputtering was performed in the sputter deposition chamber with a base pressure of 1 x 10^{-7} Torr. Sputter deposition was accomplished using a planar magnetron sputtering source (Mini Mak) operated in constant power mode of 150 Watts and an operating pressure of 15 millitorr of Argon. Argon of 99.999% purity and a copper target of 99.999% purity were used for sputter deposition.

The sample, obtained from Motorola Inc., consisted of a 1 cm^2 500 Å thick TaSiN film on a 1000 Å thick SiO_2 film grown on a Si(100) wafer. The sample was rinsed with ethanol and de-ionized water and placed into the UHV analysis chamber. X-ray photoelectron spectra of the sample were then acquired to determine the chemical composition of the air-exposed sample surface. The sample was then transferred into the deposition chamber where magnetron sputtering of copper onto the sample was performed. Target to substrate distances were such that deposition rates of ~ 0.1 Å/min were achievable, allowing a study of the film/substrate interface. Temperatures were monitored by a chromel-alumel thermocouple spot-welded between a thin titanium foil and the sample.

3.3 Results

3.3.1. Characterization of Oxidized TaSiN

X-ray photoelectron spectra for O/TaSiN are shown in Figures 3.1-3.4. As shown in Figures 3.1-3.4, spectra are acquired with the plane of the sample surface at 30° and 90° relative to the analyzer. At 90° with respect to the analyzer (surface normal), the signal from the bulk is maximized. At 60° with respect to surface normal (grazing incidence), the signal from the surface is enhanced relative to the bulk. The analysis depth, d can be estimated from

$$d = \lambda \sin\theta, \qquad (3\text{–}2)$$

where λ is the inelastic mean free path and θ is the take-off angle of the analyzed electrons [9]. Assuming the sampling depth to correspond roughly to the mean free path for the tantalum $4f_{7/2}$ photoelectron line, the sampling depth corresponds to 18 Å at surface normal and 9 Å in the grazing incidence [14]. A comparison of O/TaSiN (Table 3.1) to the sputter-cleaned TaSiN (Table 3.2) reveals the effect of the ambient on the surface of TaSiN. Exposure to the ambient results in a silicon and oxygen rich surface or, conversely, a film depleted of tantalum and nitrogen as observed in the grazing incidence data (Table 3.1). Hydrocarbon contamination served as a reference for charge calibration and was set to 285.0 eV [10]. The carbon contamination levels are presented in Table 3.1. A FWHM of 2.5 eV of the O(1s) transition of the O/TaSiN sample (Figure 3.1) indicates the presence of multiple chemical environments, since the presence of a single environment O(1s) transition present in SiO_2 is well fit with a FWHM of 2.1 eV. The experimental

Table 3.1. Atomic Composition of O/TaSiN.

	Surface Normal	Angle Resolved
Ta	19.0 %	10.7 %
Si	10.6 %	17.4 %
N	8.4 %	3.4 %
C	15.0 %	29.0 %
O	47.0 %	39.5 %

O(1s) spectrum of O/TaSiN is well fit by two components, each with a FWHM of 2.1 eV at binding energies of 530.4 eV and 532.1 eV. The component at 530.4 eV is assigned to oxygen in a metal oxide environment and the component at 532.1 eV assigned to a Si-O bond [9,15]. Silicon hydroxyls have characteristic binding energies above 533.0 eV and were not observed [15]. The O(1s) binding energies of metal hydroxides fall in the range from 531 eV to 532 eV and could not be ruled out by this fitting procedure, but their inclusion does not result in a significantly better fit [9]. Therefore, we are unable to characterize the extent to which the surface may or may not be hydroxylated. The grazing incidence O(1s) spectrum in Figure 3.1b indicates an increase in the relative intensity of the component at 532.1 eV and corresponds to the increase in oxidized silicon in the surface region (Table 3.1). The N(1s) spectrum (Figure 3.2a) partially overlaps the Ta($4p_{3/2}$) photoelectron line but exhibits a peak at 396.5 eV that is evidence of nitride formation [9]. The amount of nitride present in the

oxidized region of the sample is diminished with respect to the bulk film, which can be seen by comparison of the surface

Table 3.2. Atomic Composition of Sputter-cleaned TaSiN.[a]

	Surface Normal
Ta	56.3 %
Si	10.1 %
N	23.3 %
O	10.3 %

[a] Preferential sputtering of the lighter elements may have occurred.

normal (Figure 3.2a) and grazing incidence spectra (Figure 3.2b). The Ta(4f) spectra in Figures 3.3a of O/TaSiN include both the Ta($4f_{7/2}$) and the Ta($4f_{5/2}$) photoelectron lines, which are present in a 4:3 intensity ratio, respectively with a 1.9 eV separation [9]. The binding energies reported here refer to the Ta($4f_{7/2}$) photoelectron line. The Ta(4f) doublet at 26.1 eV is well fit with a FWHM of 1.8 eV for each component. This distinctive doublet at 26.1 eV is assigned to a TaO_x species. The relative intensity of this component is increased at grazing incidence, as is consistent for an oxidized film (Table 3.1). Tantalum pentoxide and tantalum silicide were considered, but eliminated as possible candidates in the oxidized sample, since these species have higher binding energies occurring at 26.5 eV and 26.9 eV, respectively [16,17]. The second distinctive doublet in Figure 3.3a occurring at a binding energy of 22.4 eV is fit by using a weighted spectrum

(background corrected) of sputter-cleaned tantalum silicon nitride to facilitate inclusion of the asymmetrical lineshape (Figure 3.3b). The Si(2p) spectrum of oxidized TaSiN in

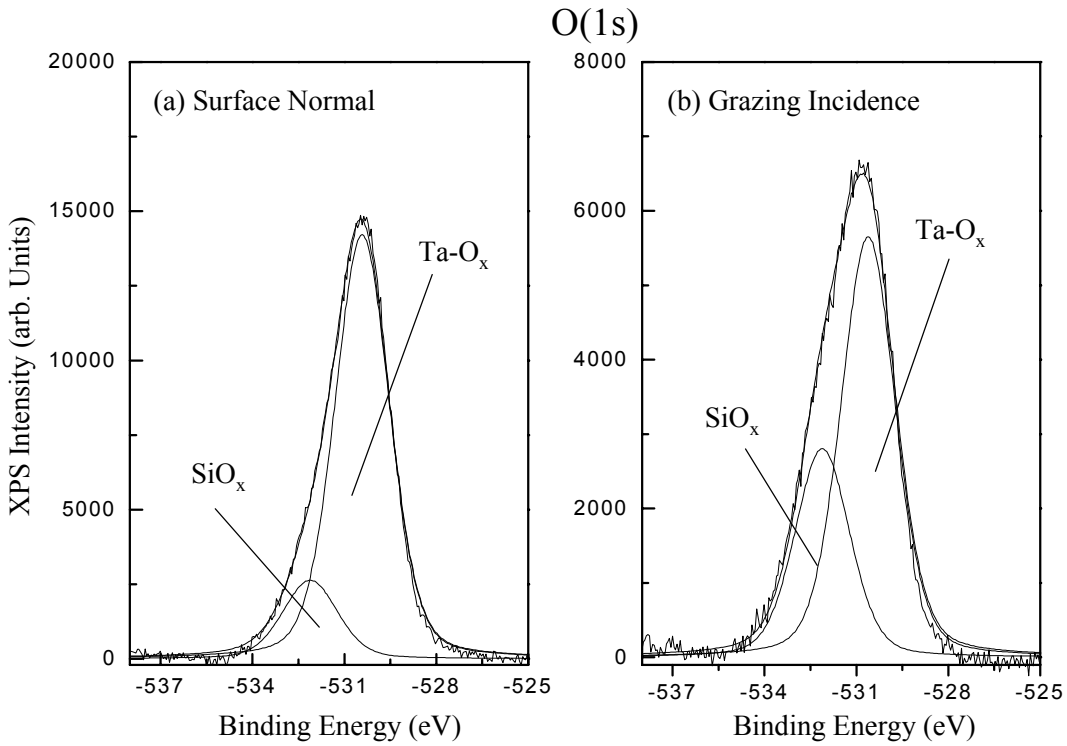

Figure 3.1. XPS O(1s) spectra of O/TaSiN. (a) Surface Normal. (b) Grazing Incidence.

Figure 3.4a has two well-resolved components. The FWHM of the Si(2p) transition is 2.3 eV, which matches the Si(2p) photoelectron line for the single environment in SiO_2. The binding energy component at 102.0 eV is assigned to silicon in SiO_x [18]. Silicon dioxide was considered, but eliminated as a possible candidate having a higher binding energy occurring at 103.6 eV [18]. The peak at 98.6 eV is assigned to silicon in the TaSiN environment by comparison with sputter-cleaned TaSiN (Figure 3.4b).

In summary, the spectra in Figures 3.1-3.4 along with the calculated compositions of O/TaSiN (Table 3.1) and sputter-cleaned TaSiN (Table 3.2) films indicate that the

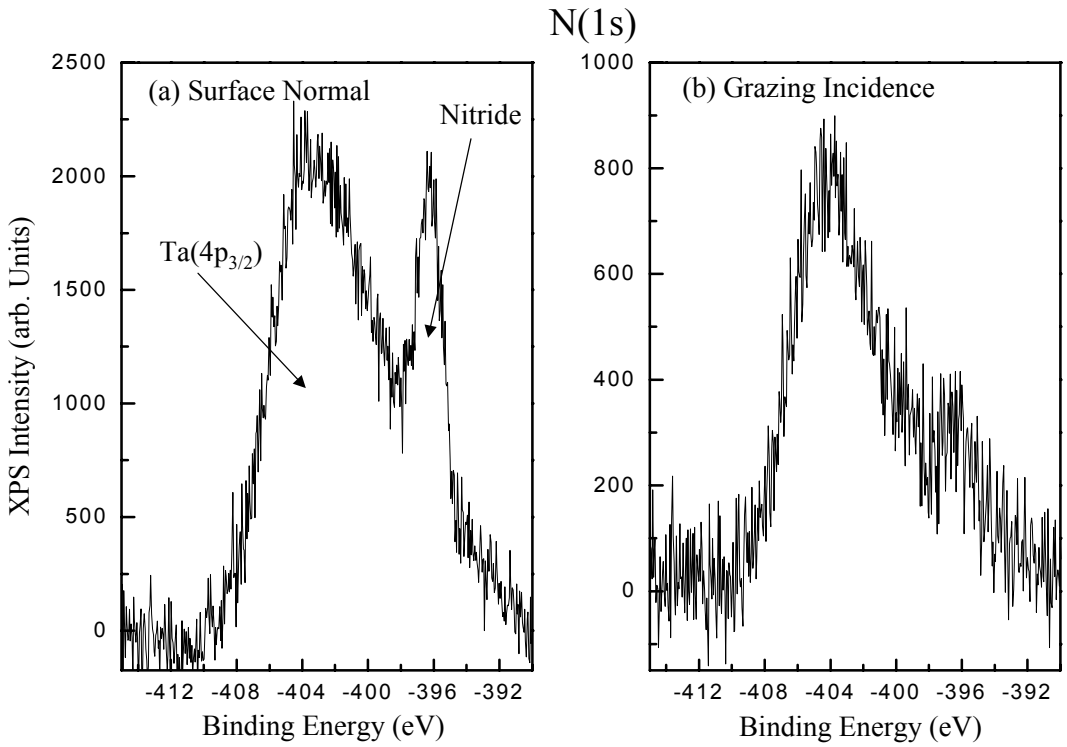

Figure 3.2. XPS N(1s) spectra of O/TaSiN. (a) Surface Normal. (b) Grazing Incidence.

exposure of TaSiN to the atmosphere results in the oxidation of the near surface region and the consequent depletion of N in that region. The XPS data indicate a thin (~ 10Å) layer of a SiO_x and TaO_x species, with a Si/Ta atomic ratio ~ 2.

3.3.2 Cu/O/TaSiN

Cu was sputter deposited onto O/TaSiN in sequential depositions of 120 sec. each. After each deposition, the sample was transferred from the sputter deposition chamber to

the UHV chamber for XPS analysis, and then back to the sputter deposition chamber for additional depositions. The Cu(L_3VV) Auger lineshape (x-ray excited), displayed in

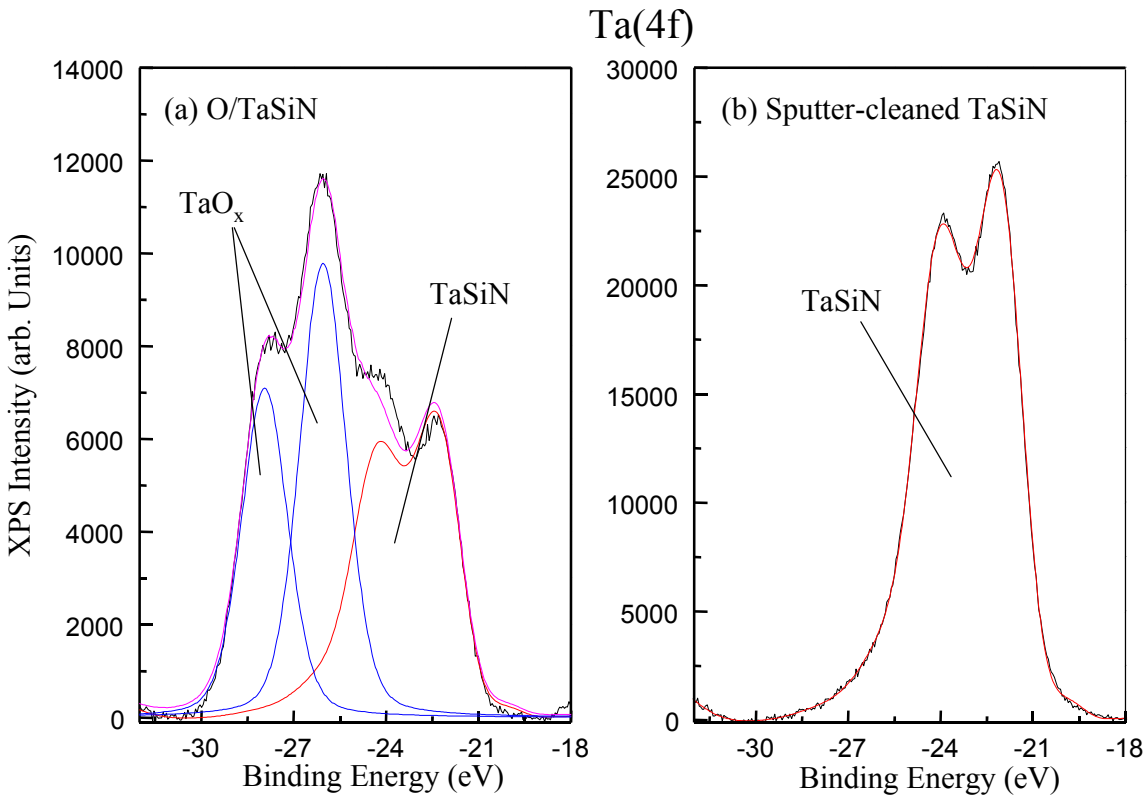

Figure 3.3. XPS Ta(4f) spectra. (a) O/TaSiN. (b) TaSiN.

Figure 3.5a, provides a "fingerprint" of the oxidation state of the deposited Cu on O/ TaSiN [19]. The oxidation state of the Cu evolves with deposition time from Cu(I) to Cu(0). The feature at 914.9 eV (Figure 3.5a) is associated with the presence of Cu(I), whereas the feature at 917.6 eV is indicative of Cu(0) [20-22]. A modified Auger parameter {α = KE of Cu(L_3VV) maximum + BE of Cu($2p_{3/2}$)} is calculated for the conditions

under which only Cu(I) is present [23,24]. The calculated Auger parameter with only Cu(I) present (depositions 1-5) is 1847.8 eV. An Auger parameter value of 1847.8 eV is in the range of Auger parameters reported for other Cu(I) compounds [9]. The Auger parameters

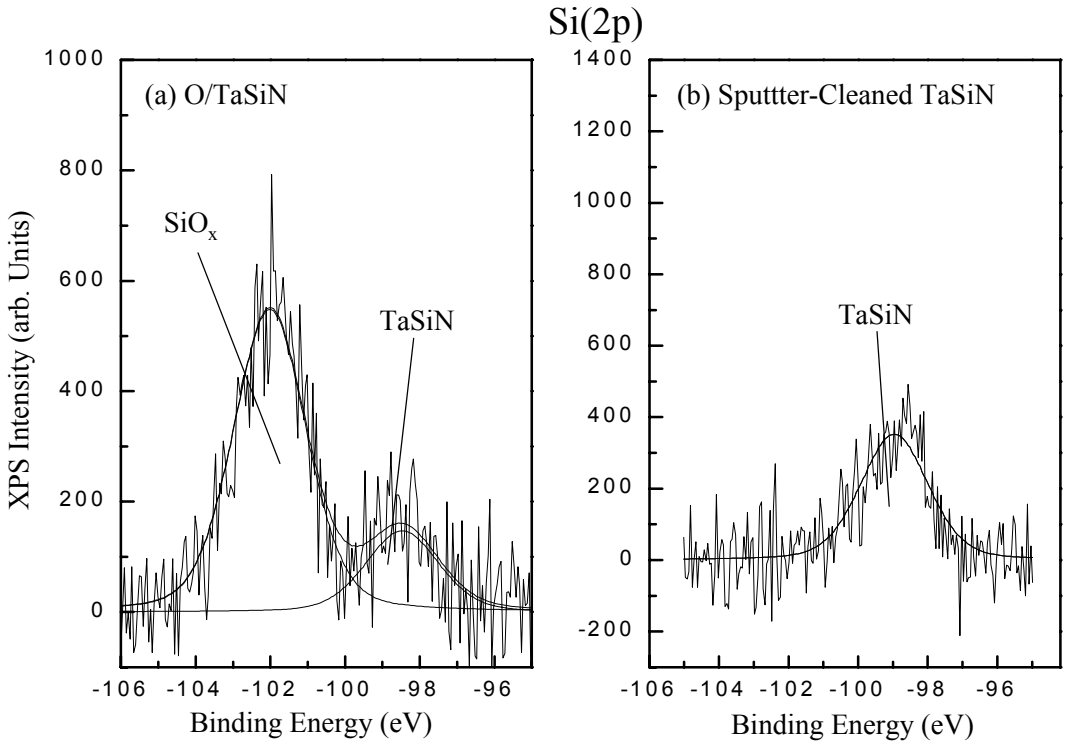

Figure 3.4. XPS Si(2p) spectra. (a) O/TaSiN. (b) TaSiN.

with Cu(I) and Cu(0) both present, corresponding to 18 min of deposition, are 1847.8 eV and 1850.4 eV, respectively (Figure 3.5a). The Auger parameter value of 1850.4 eV is lower than that reported for bulk Cu which is 1851.3 eV [9]. Experiments performed by Wu *et al*. for copper on Al_2O_3 also report lower Auger parameters than those found in bulk copper [25]. In the paper, Wu attributes the low Auger parameters to be a result of

ineffective screening that occurs for metallic copper coverages of 0.5 Å average thickness [25].

Copper depositions 1-5 (Figure 3.5a) on O/TaSiN yield a Cu(L_3VV) Auger lineshape indicative of Cu(I), with a single peak at 914.9 eV [20,21]. After the sixth and

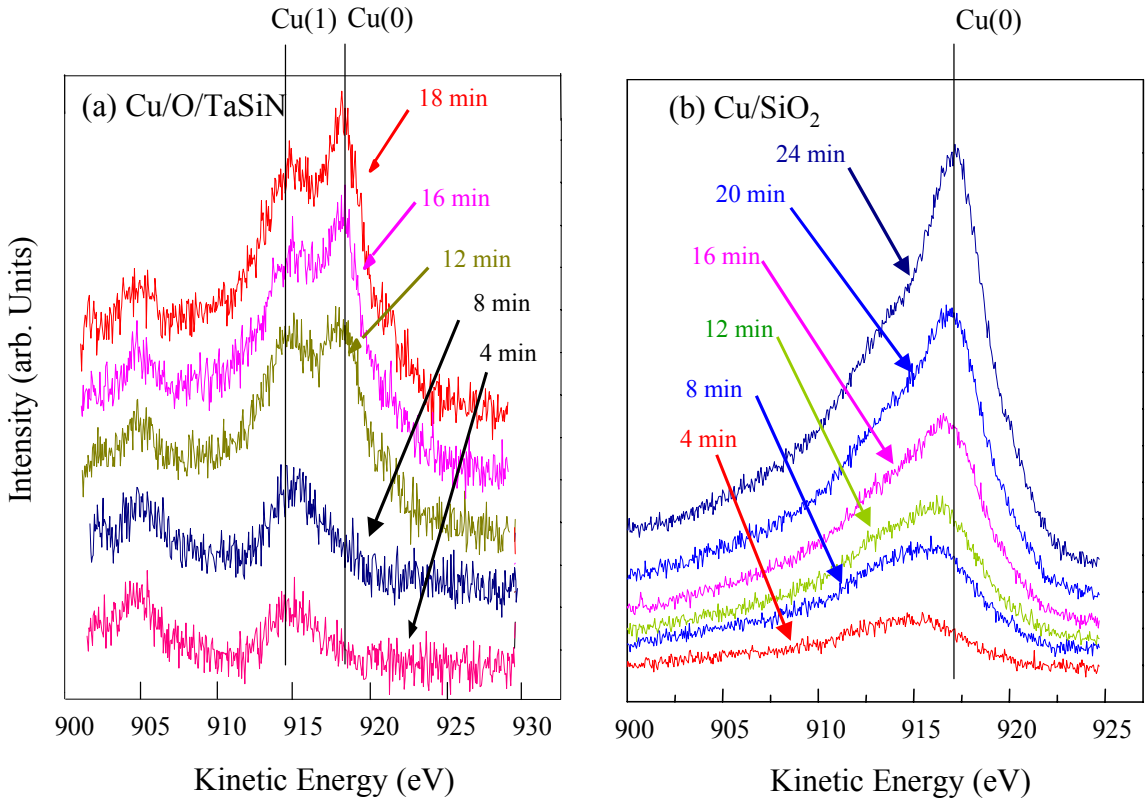

Figure 3.5. X-ray excited Cu(L_3VV) Auger spectral evolution as a function of deposition time. (a) Cu/O/TaSiN. (b) Cu/SiO_2.

subsequent depositions O/TaSiN film (Figure 3.5a), the growth of another feature at 917.6 eV Auger kinetic energy is observed, indicating the formation of Cu(0) [22]. These data for O/TaSiN indicate that, upon the sixth and subsequent depositions, substrate sites are not available for reaction with deposited Cu, and Cu-Cu interactions dominate.

Copper depositions carried out under identical conditions on SiO_2 result in only Cu(0) formation (Figure 3.5b). Copper behavior on SiO_2 is of relevance because of the large composition of silicon and oxygen in the O/TaSiN film(Table 3.1). The data for SiO_2 contrast data for O/TaSiN, where copper does "wet" the substrate.

The mode of growth of the Cu overlayer on a substrate can be characterized by plotting the increase in Cu intensity (relative to O) as a function of deposition time [26]. Figures 3.6a and 3.6b include the mode of growth of Cu on O/TaSiN and SiO_2, respectively. Cu/O XPS intensity error bars arising from deviations from the average of the intensities are determined to be less than 6 %. The linearity observed for Cu on SiO_2 indicates that copper deposition occurs with the formation of 3-dimensional islands [15]. The nonlinearity at very low coverages, previously reported by J.B. Zhou *et al*. and attributed to an anomously low Cu sticking coefficient on SiO_2 was not observed [27]. The difference may be an effect of sputter deposition versus thermal evaporation. In contrast to the behavior of Cu on SiO_2, the mode of growth of Cu on O/TaSiN is characterized by a change in slope for 5th and subsequent depositions (Figure 3.6a). The change in slope in Figure 3.6a along with the data in Figure 3.5a is indicative of conformal growth of an initial Cu(I) ad-layer [14,28]. The change in slope (Figure 3.6a) coincides with the initial formation of Cu(0) in Figure 3.5a. Plots of Cu/Si and Cu/Ta XPS Intensity vs. Deposition Time yield identical breaks. The results indicate no preferential attenuation of TaO_x or SiO_x. For the purpose of describing copper "wetting" behavior, the oxide surface is laterally homogeneous. The surface coverage of Cu(I) at the break cannot be precisely

determined because of the complex composition of the surface region but can be approximated as follows. In order to calculate the Cu/O ratio, the fraction of oxygen intensity from the first atomic layer must be known. The fraction of oxygen intensity

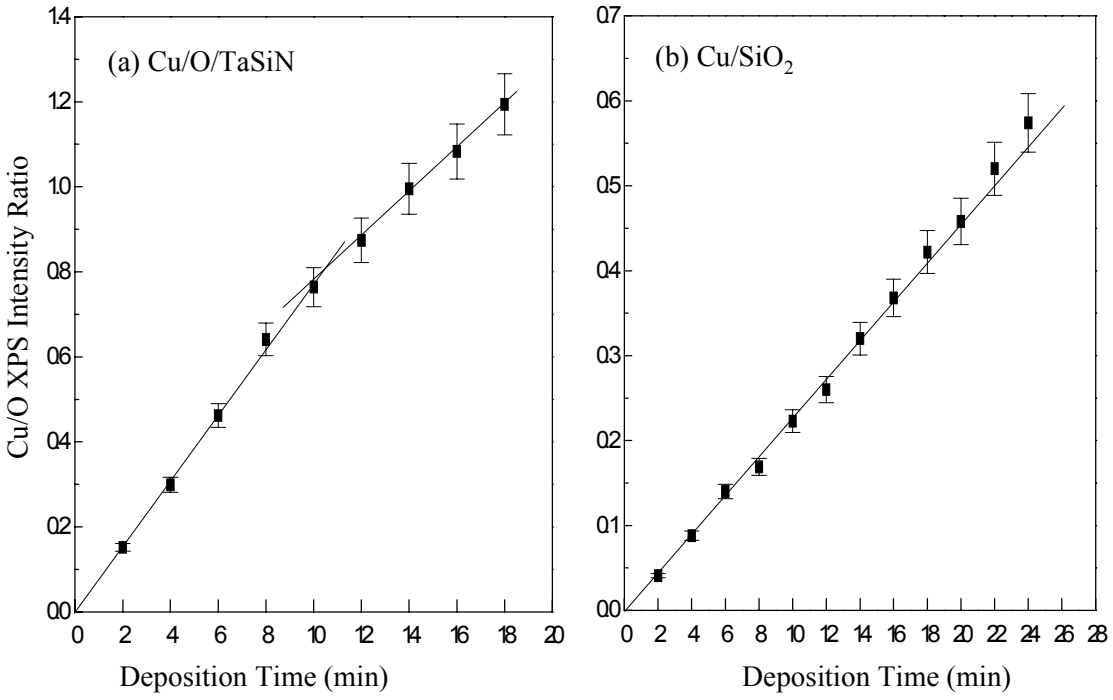

Figure 3.6. Uptake Curves for (a) Cu/O/TaSiN. (b) Cu/SiO_2.

originating from the first atomic layer can be estimated with the following equation:

$$\text{Fraction of Oxygen Intensity from First Atomic Layer} = \frac{\int_0^1 \exp(-x/\lambda)\,dx}{\int_0^\infty \exp(-x/\lambda)\,dx}, \qquad (3\text{–}3)$$

where λ is the mean free path in monolayers. A mean free path of 5.8 ML for the O(1s) photoelectron is obtained from the universal curve [29]. Equation (3-3) yields the result that

16 % of the total oxygen intensity is contributed by the first atomic layer of the substrate. The copper coverage (on a Cu/O atomic basis) can now be calculated from the following expression:

$$Cu / O = I_{Cu}A_O / 0.16 I_O A_{Cu} \quad (3\text{-}4)$$

The copper coverage at the break (Figure 3.6a) is 0.40 ML (based on the copper to oxygen atomic ratio), which allows as a rough estimate of the total copper coverage. A Cu(I) coverage of ~ 0.40 ML is consistent with an ionic Cu adlayer, with coverage limited by repulsive Cu(I)-Cu(I) interactions. Similar effects have been observed for Cu on aluminum oxide surfaces [30]. The data in Figures 3.5 and 3.6 combine to indicate that Cu is deposited conformally and reacts with the oxidized substrate to form a Cu(I) film in the first ad-layer followed by Cu(0) formation.

3.3.3 Thermal Stability of Copper on Oxidized TaSiN

With a copper coverage ~ 0.60 ML (Cu(I) and Cu(0) present), the O/TaSiN sample is annealed to sequentially higher temperatures with annealing periods of 6 minutes at each temperature. Annealing of the copper sputtered sample results in a decrease in copper to oxygen XPS intensity ratios as shown in Figure 3.7. The largest decreases in Cu/O XPS intensity occur in the 500 K to 800 K region.

Along with the decrease in the Cu/O XPS intensity ratios, a change in the oxidation state of copper is observed upon annealing. After a 16 minute sputter deposition at 300 K, copper is present as Cu(I) and as Cu(0) as indicated in Figure 3.8a,

with features at 914.9 eV and 917.6 eV, respectively [20,21]. As the sample is annealed to 600 K, a significant change occurs in the Cu(L_3VV) lineshape. Copper is now present

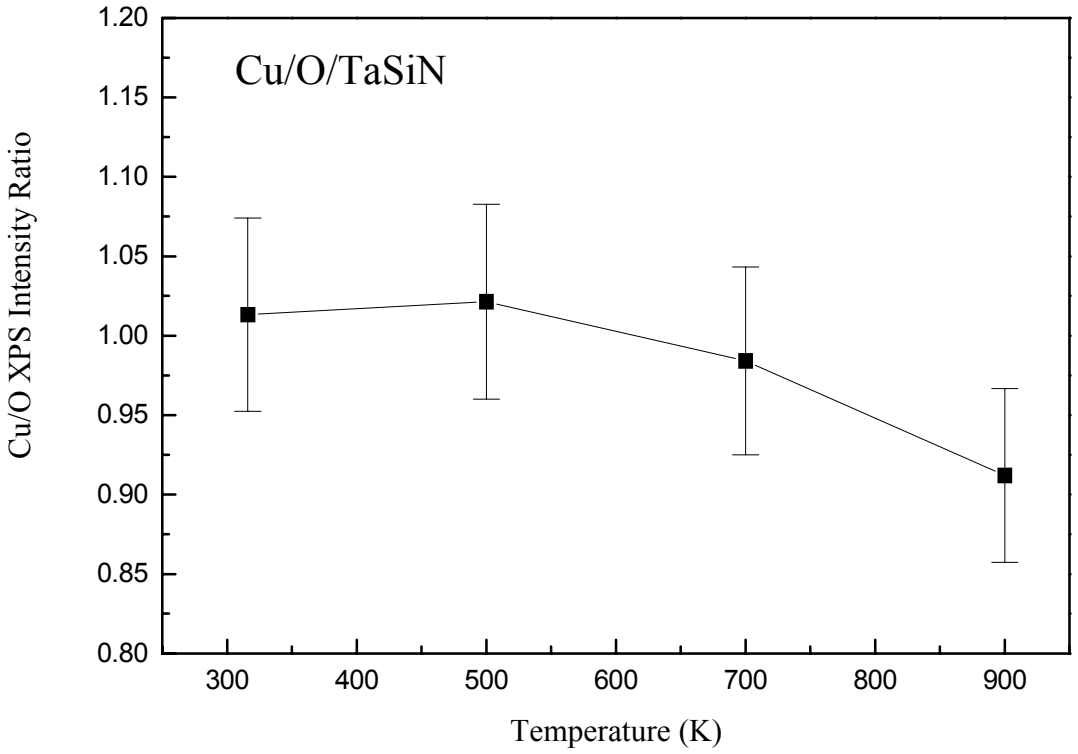

Figure 3.7. Relative Cu intensity vs. annealing temperature for Cu on O/TaSiN.

predominantly as Cu(0) as evidenced by the dominant feature at 917.6 eV in Figure 3.8b [23]. Annealing to temperatures up to 900 K (Figure 3.8c) yields no further changes in the lineshape of the Cu(L_3VV).

The possibility of diffusion was examined for temperatures up to 900 K. The O/TaSiN sample was subject to annealing up to 900 K until no further decrease in Cu($2p_{3/2}$) signal could be observed. If diffusion had occurred, the copper on the surface

and the copper in the film should then be in equilibrium. Next, sputtering cleaning of the surface was then performed to remove Cu from the surface. The sample was then

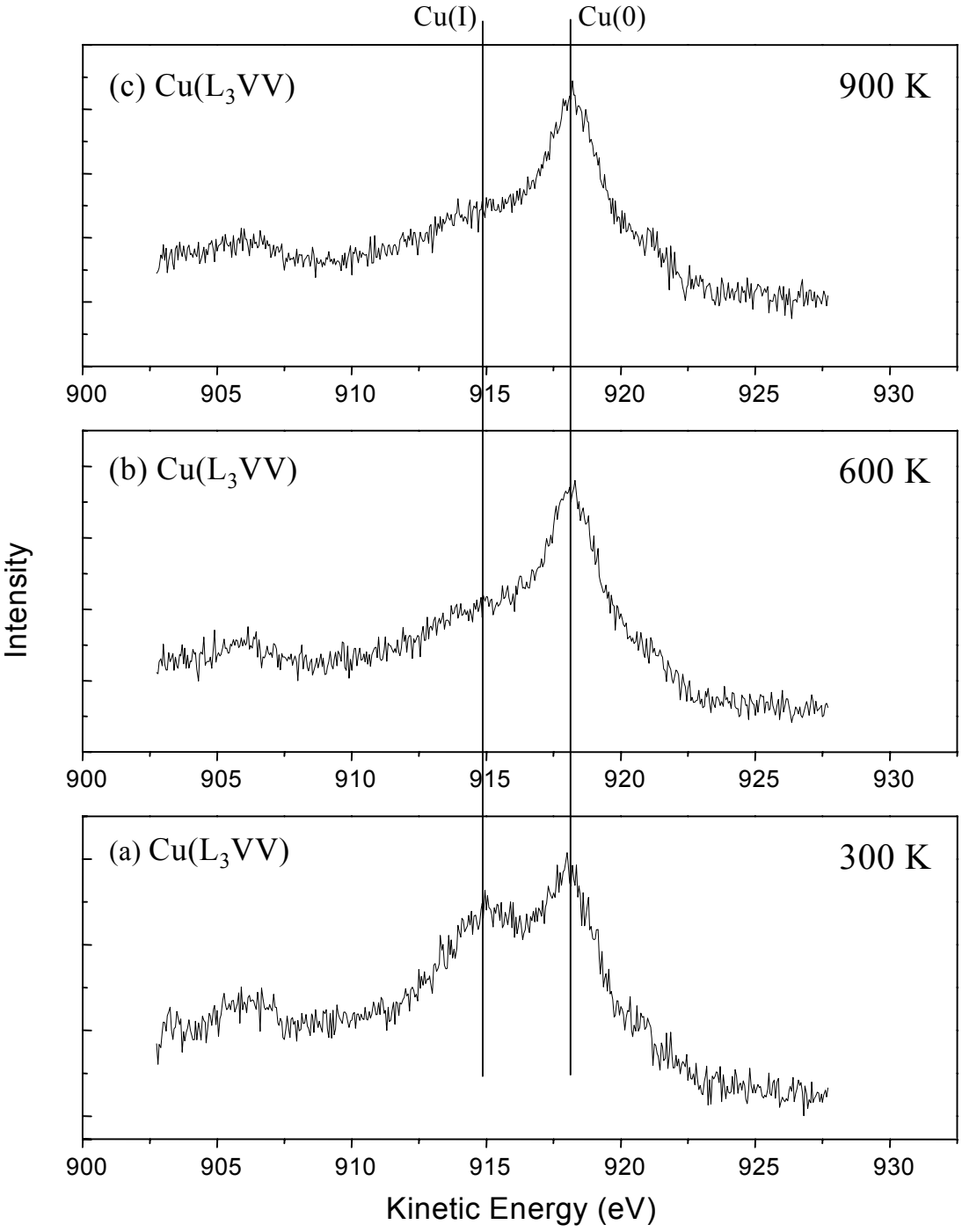

Figure 3.8. X-ray excited Cu(L_3VV) Auger spectra after annealing. (a) 300 K. (b) 600 K. (c) 900 K.

annealed again to see if any copper would segregate from the bulk. No copper was found to segregate to the surface. This case is in contrast with results obtained on clean TaN (Chapter 2), where copper did indeed segregate from the bulk to the surface. With the oxidized layer only about 10 angstroms deep, it was not possible to eliminate the possibility of copper diffusing through the thin oxidized layer to the oxide/substrate interface. However, diffusion of copper past this layer was not observed as evidenced by the absence of copper segregation from the bulk to the sputter cleaned surface. This data corroborates measurements performed by Nicolet *et al*. that copper does not diffuse into clean TaSiN up to 1100 K [6,31].

3.4. Discussion

The data presented above demonstrate that copper reacts with O/TaSiN in the first ad-layer and forms Cu(I) at 300 K to a maximum coverage of 0.4 ML (on a Cu/O atom basis). At higher coverages, Cu(0) is formed. The behavior of Cu on O/TaSiN (Figures 3.5a & 3.6a) can be compared with Cu/SiO_2 (Figures 3.5b & 3.6b). Copper interacts only weakly with the SiO_2 surface, readily forming Cu(0) [27]. Copper uptake curves on SiO_2 do not display the sharp change in slope (Figure 3.6b) which is characteristic of layer-by-layer growth,[14] *i.e.* copper does not "wet" SiO_2 at 300 K. In contrast to Cu/SiO_2, Cu/O/TaSiN displays initial conformal growth with formation of Cu(I). This

demonstrates significant charge exchange between the initial Cu ad-atoms and the substrate. This also demonstrates, that although the surface region of O/TaSiN is enriched in silicon and oxygen, the surface layer itself is not SiO_2. The possibility of segregated surface regions of SiO_x and TaO_x may be discarded since one would expect preferential attenuation of either the Si or Ta XPS intensities. These results indicate that the composition of the O/TaSiN surface is a relatively homogeneous $Ta_xSi_yO_z$ mixture.

Annealing of the conformally deposited Cu ad-layer to temperatures above 500 K in UHV results in a decrease in the Cu/O intensity ratios. The decrease in relative Cu signal intensity is due to the formation of 3-dimensional nuclei on the surface due to the "de-wetting" of the Cu from the oxidized surface at elevated temperatures. As copper "de-wets", more of the substrate is exposed, causing an increase in the tantalum signal. Furthermore, copper attenuates its own signal by shielding of the copper atoms inside the 3-D islands. At a temperature sufficiently large for a Cu atom to overcome the chemisorption energy well and become mobile on the surface, Cu-Cu interactions would dominate. The results show that although diffusion of copper does not occur for temperatures less than 900 K, annealing of the Cu ad-layer above 500 K in UHV causes "de-wetting" of Cu from the O/TaSiN.

It is of interest to contrast the behavior of O/TaSiN with that of TiO_2. The case of TiO_2 is relevant to TiN because TiN exposed to air has a TiO_2 surface layer [32]. The copper "wetting" and adhesion to oxidized TiN is notoriously poor [33]. The poor adhesion between copper and TiO_2 is connected with the lack of electron transfer between the

copper and TiO_2, i.e., copper is present as Cu(0) even at low coverages [35]. The results reported here for Cu on O/TaSiN, compared to those observed for Cu on oxidized TiN, indicate stronger interactions between Cu and O/TaSiN.

3.5 Conclusions

Copper is sputter-deposited onto O/TaSiN. The exposure of TaSiN to the atmosphere results in an oxygen rich, tantalum and nitrogen depleted region of 10 Å. The data indicate the surface to be a homogeneous $Ta_xSi_yO_z$ mixture rich in silicon. Copper sputter deposited onto O/TaSiN results in copper "wetting" of the surface and is characterized by a feature in the Cu(L_3VV) Auger lineshape at 914.9 eV indicative of Cu(I) [20,21]. Further deposition of the copper results in the addition of a new feature in the Cu(L_3VV) Auger lineshape at 917.6 eV and is indicative of Cu(0) [23]. These data indicate that copper initially deposited reacts and forms Cu(I) for the first ad-layer. Subsequent copper deposition results in Cu(0) formation. Annealing experiments performed reveal that although diffusion is not observed for temperatures less than 900 K, copper "de-wetting" occurs ~ 500 K.

3.6. Chapter References

[1] Pai, P. C.; Ting, C. H. *IEEE Electron Device Lett.* **1989**, *10*, 423.

[2] Nicolet, M.-A.; Suni, I.; Finetti, M. *Solid State Technol.* **1983**, *26*, 129.

[3] Wiley, J. D.; Perpezko, J. H.; Nordman, J. E.; Gus, K. J. *IEEE Trans. Ind. Electron.* **1982**, *IE-29*, 154.

[4] Hung, L. S.; Saris, F. W.; Wang, S. Q.; Mayer, J. W. *J. Appl. Phys.* **1986**, *59*, 2416.

[5] Angyal, M. S.; Shacham-Diamand, Y.; Reid, J. S.; Nicolet, M.-A. *Appl. Phys. Lett.* **1995**, *67*, 2152-2154.

[6] Kolawa, E.; Pokela, P. J.; Reid, J. S. *IEEE Electron Device Letters* **1991**, *12*, 321-323.

[7] Reid, J. S.; Kolowa, E.; Ruiz, R. P.; Nicolet, M.-A. *Thin Solid Films* **1993**, *236*, 319-324.

[8] Guinn, K. V.; Donnelly, V. M.; Gross, M. E.; Baiocchi, F. A.; Petrov, I.; Greene, J. E. *Surface Science* **1993**, *295*, 219-229.

[9] Moulder, J. F.; Stickle, W. F.; Sobol, P. E.; Bomben, K. D. *Handbook of X-ray Photoelectron Spectroscopy*; Moulder, J. F.; Stickle, W. F.; Sobol, P. E.; Bomben, K. D., Ed.; Physical Electronics, Inc.: Eden Prarie, Minnesota, 1992.

[10] Beamson, G.; Briggs, D. *High Resolution XPS of Organic Polymers: The Scienta ESCA300 Database*; Beamson, G.; Briggs, D., Ed.; John Wiley & Sons: New York, New York, 1992, pp 26.

[11] *ESCA Tools*; 4.6 ed.; Surface/Interface Inc., Mountain View, CA., 1995.

[12] Shirley, D. A. *Phys. Rev. B* **1972**, *5*, 4709.

[13] Sherwood, P. M. A. *J. Vac. Sci. Technol. A* **1995**, *14*, 1424.

[14] Somorjai, G. A. *Introduction to Surface Chemistry and Catalysis*; Somorjai, G. A., Ed.; John Wiley & Sons: New York, New York, 1994, pp 667.

[15] Miller, M. L.; Linton, R. W. *Anal. Chem.* **1985**, *57*, 2314.

[16] Sarma, D. D.; Rao, C. N. R. *J. Electron Spectrosc. Relat. Phenom.* **1980**, *20*, 25.

[17] Mcguire, G. E.; Schweitzer, G. K.; Carlson, T. A. *Inorg. Chem.* **1973**, *12*, 2451.

[18] Hollinger, G. *Appl. of Surf. Sci.* **1981**, *8*, 318.

[19] Nuesca, G. M.; Kelber, J. A. *Thin Solid Films* **1995**, *262*, 224-233.

[20] Wagner, C. D. *Discuss. Faraday Soc.* **1975**, *60*, 291.

[21] Klein, J. C.; Proctor, A.; Hercules, D. M.; Black, J. F. *Anal. Chem* **1983**, *55*, 2055.

[22] Kowalczky, S. P.; Pollak, R. A.; McFeely, F. R.; Ley, L.; Shirley, D. A. *Phys. Rev. B* **1973**, *8*, 2387.

[23] Wagner, C. D.; Gale, L. H.; Raymond, R. H. *Anal. Chem.* **1979**, *151*, 466.

[24] Garenstroom, S. W.; Winograd, N. *J. Chem. Phys.* **1977**, *67*, 3500.

[25] Wu, Y.; Garfunkel, E.; Madey, T. E. *J. Vac. Sci. Technol. A* **1996**, *14*, 1662-1667.

[26] Stampanoi, M.; Vaterlans, A.; Aeschlimann, M.; Pescia, D. *J. Appl. Phys.* **1988**, *64*, 5321.

[27] Zhou, J. B.; Lu, H. C.; Gustaffson, T. *Surface Science Letters* **1993**, *293*, L887-L892.

[28] Peden, C. H. F.; Kidd, K. B.; Shinn, N. D. *J. Vac. Sci. Technol. A* **1991**, *9*, 1518-1523.

[29] Seah, M. P. *Practical Surface Analysis*; 2nd ed.; Seah, M. P., Ed.; John Wiley & Sons: New York, 1990; Vol. 1, pp 207.

[30] Varma, S.; Chottiner, G. S. *J. Vac. Sci. Technol. A* **1992**, *10*, 2857.

[31] Kolawa, E.; Chen, J. S.; Reid, J. S.; Pokela, P. J.; Nicolet, M.-A. *J. Appl. Phys.* **1991**, *70*, 1369-1373.

[32] Prasad, J.; Nuesca, G.; Kelber, J. A. *Appl. Surf. Sci.* **1994**, *74*, 115.

[33] Kim, D. H.; Wenterof Jr., R. H.; Gill, W. N. *J. Appl. Phys.* **1993**, *74*, 5164.

CHAPTER 4

BEHAVIOR OF Cu(60 %)Al(40%) FILMS AT THE SILICON DIOXIDE INTERFACE

4.1. Introduction

Copper-aluminum alloys have been proposed as self-developing barriers in ultra large scale integration (ULSI) and gigascale intergration (GSI) manufacturing [1]. With the miniaturization of microelectronic devices, RC delays in interconnects necessitate the replacement of aluminum with copper. Copper is lower in resistivity and offers a greater resistance to electromigration than aluminum [2,3]. Copper integration as an interconnect material poses several problems, however. These problems include the poor adhesion of copper to SiO_2 and the rapid diffusion of copper through SiO_2. Studies performed by Murarka *et al*. report promising results for 1000 Å and 5000 Å Cu(Al) films (0.5-1.0 at. % Al) deposited on SiO_2 with good electrical (capacitance-voltage and current-voltage) properties and better adhesion (Scotch tape tests) than Cu on SiO_2 [4, 5]. It has been suggested that annealing of these Cu(Al) films in vacuum results in migration of aluminum to the SiO_2 interface resulting in the formation of a thin oxide layer that enhances the adhesion of copper to the dielectric [4]. These findings indicate that further research is required in this area, especially as it relates to the adhesion and diffusion characteristics of copper-aluminum films at SiO_2 interface.

APPENDIX

Abbreviations

XPS X-ray Photoelectron Spectroscopy

ML Monolayer

SEM Scanning Electron Microscopy

ULSI Ultra Large Scale Integration

GSI Gigascale Integration

VLSI Very Large Scale Integration

VM Volmer-Weber mode

SK Stranski-Krastanov mode

FM Frank-van der Merwe mode

CVD Chemical Vapor Deposition

PVD Physical Vapor Deposition

ESCA Electron Spectroscopy for Chemical Analysis

UHV Ultra High Vacuum

EDX Energy Dispersive X-ray Analysis

FWHM Full Width Half Max

MOSFET Metal Oxide Field Effect Transistor

Although the ability of copper to "wet" or adhere to SiO_2 has been well-studied, the interaction of Cu(Al) films at the SiO_2 interface remains largely unexplored. In our study, we use a CuAl (40 at % Al) target to deposit high aluminum content films relative to the studies performed by Murarka *et al* [4,5]. The reasons for this are two-fold. First, the deposition of Cu(Al) films (~ 1-3 ML) with higher aluminum content allows the simulation of the aluminum-rich interface that occurs upon annealing of the Cu(Al) films (0.5-1 at. %) [4]. Second, the deposition of Cu(Al) films with high aluminum content enables us to determine the composition of these films using XPS, since lower aluminum compositions would be obscured by the overlap of the Cu(3p) and Al(2p) regions in the XPS spectra. In this study, we contrast the wetting behavior and thermal stability of $Cu_{0.6}Al_{0.4}/SiO_2$, Cu/SiO_2 and Cu/α-$Al_2O_3(0001)$ (sapphire).

4.2. Experimental Methodologies

XPS and sputter deposition experiments were performed in an ultra high vacuum (UHV) system described in Section 1.5.2. [6]. The sputter deposition chamber had a base pressure of 1×10^{-8} Torr, while the XPS analysis chamber had a base pressure of 5×10^{-10} Torr. Spectra were obtained using an unmonochromatized MgKα x-ray source (PHI model 1427) operated at 15 keV and 300 Watts and a hemispherical analyzer (VG100AX) operated in the constant pass energy mode (50 eV). Collected data were referenced to an energy scale calibrated with binding energies of Au($4f_{7/2}$) at 84.0 eV and Cu($2p_{3/2}$) at 932.7 eV [7]. The observed binding energies were affected by sample charging during acquisition. Differential charging was determined not to have occurred since the

separation between the Si(2p) and O(1s) photoelectron lines was 429.5 eV, which corresponds to the expected separation between the Si(2p) and O(1s) photoelectron lines [8]. Therefore, the Si(2p) binding energy of SiO_2 was set to 103.6 eV [8] and used as a reference for the calibration of other peak positions. Grazing incidence spectra were obtained by rotating the sample 60° off surface normal and XPS data analysis was performed using commercially available software (ESCA Tools) [9]. Peak fitting was accomplished using Guassian-Lorentzian functions. Shirley background subtraction, a well-established subtraction method for small energy windows found in typical core level XPS spectral synthesis, was adopted in this study [10,11]. Atomic concentrations were calculated with atomic sensitivity factors specific for the hemispherical analyzer (VG100AX) and were obtained directly from the manufacturer.

DC magnetron sputtering was performed in the sputter deposition chamber with a base pressure of 1 x 10^{-8} Torr. Sputter deposition was accomplished using a planar magnetron sputtering source (Mini Mak) operated in constant power mode. Argon of 99.999 % purity and a Cu and CuAl (40 at. % Al) target of 99.999 % purity were used for sputter deposition. Following deposition of these films, the films were annealed at several temperatures for 20 minutes in UHV. *Ex-situ* scanning electron microscopy (SEM) images of the sample were then acquired using a JEOL JSM-T300 equipped with energy dispersive x-ray analysis (EDX) capabilities to determine the dewetting temperature of copper in these films. Air exposure prior to SEM imaging was typically under 2 hrs. The maximum resolution achievable for the JEOL JSM-T300 is 6 nm at 60 kV and a working

distance of 8 mm. The SEM micrographs in this study were taken at an accelerating voltage of 15 kV.

The silicon oxide samples used in this study were provided by Texas Instruments and consisted of 1000 Å SiO_2 grown on a Si(100) wafer. Samples (10 x 10 x 0.5 mm) of commercially obtained α-Al_2O_3(0001) were also used. Both types of samples were mounted on a tantalum sample holder and annealed in O_2 at 10^{-6} Torr at 1000 K prior to copper deposition. Temperatures were monitored by a chromel-alumel thermocouple spot-welded between a thin tantalum foil and the sample. Carbon contamination levels prior to deposition of the films were ~ 0.6 ML (based on a C/O atomic ratio). A decrease in the C/Cu XPS intensity as a function of deposition time indicates that the C intensity is attenuated by the deposited copper. The C(1s) photoelectron line binding energy of 284.8 eV indicates only adventitious carbon contamination and provides no evidence of carbide formation. Ar^+ sputter cleaning of SiO_2 was avoided so as not to create oxygen vacancy defects which could effect the wetting process. Such C contamination is in any case undoubtedly present during many industrial processes.

4.3. Results

4.3.1. XPS Characterization of Copper Aluminum Films on SiO_2

A CuAl (40 at. % Al) target was sputtered for 360 sec. at an operating pressure of 9 millitorr of Argon and 150 Watts to form sub-monolayer Cu(Al) films on SiO_2. Generally, the composition of a sputtered film resembles that of the alloy target [12]. The

composition of the Cu(Al) films deposited in this study are calculated using the following equation:

$$\frac{Cu}{Al} = \frac{I_{Cu} S_{Al}}{I_{Al} S_{Cu}} \qquad (4\text{-}1)$$

where I is the intensity of the photoelectron signal detected per second, and S is the atomic sensitivity appropriate to the analyzer [7,13]. The composition of the sputtered film was found to be $Cu_{0.6}Al_{0.4}$, by deconvolution of the XPS spectra (Figure 4.1a). The presence of aluminum in the film was also confirmed by *ex-situ* EDX. However, any quantitative analysis of the deposited film using EDX was complicated by the overlap of the Al Kα (1.44 keV) peak with the predominant Si Kα (1.74 keV) peak of the substrate.

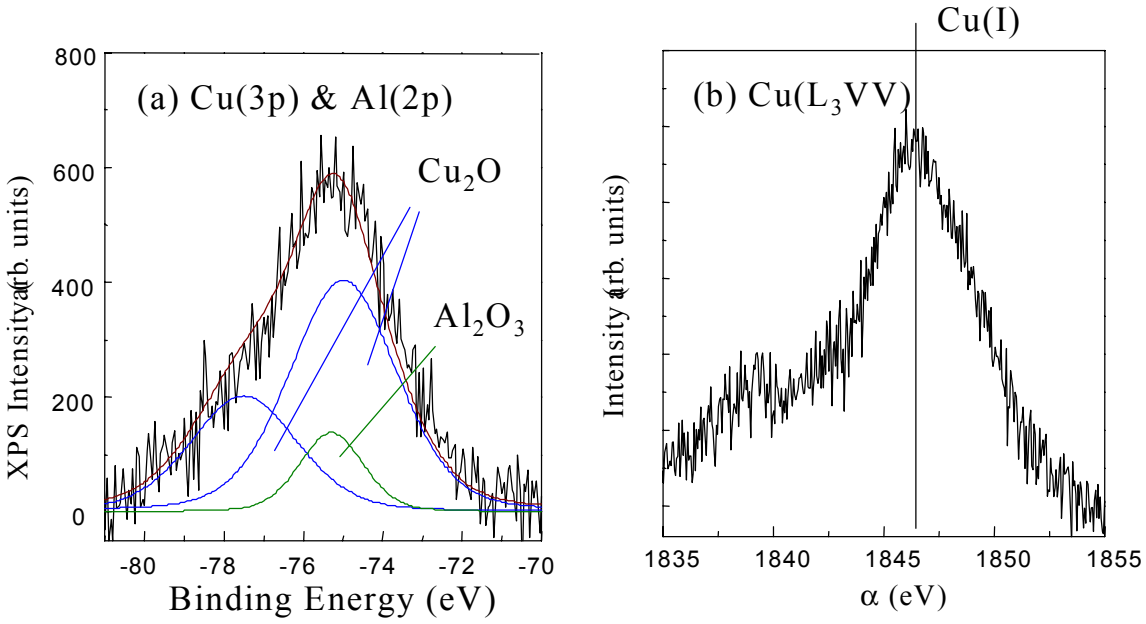

Figure 4.1. Formation of $Cu_{0.6}Al_{0.4}$ Films after 360 sec of Deposition. (a) Cu(3p) & Al(2p) Spectra. (b) X-ray Excited Cu(L_3VV) Spectra.

The spectra of the Al(2p) photoelectron line and the Cu(3p) doublet are displayed in Figure 4.1a. As evident in Figure 4.1a, there is considerable overlap of the Al(2p) and Cu(3p) regions. Quantitative analysis using the Al(2s) photoelectron line was impeded by the energy loss line from the parent Si(2p) photoelectron line which obscured the Al(2s) signal. Therefore, peak fitting of the spectra was carried out to determine the relative intensities of the Al(2p) and Cu(3p) photoelectron lines. The Cu(3p) doublet intensity ratio, peak separation and FWHM are determined by comparison to the single environment of pure metallic copper. The Cu($3p_{3/2}$) and Cu($3p_{1/2}$) photoelectron lines (Figure 4.1a) are present in a 2:1 intensity ratio, respectively and separated by 2.4 eV [14]. The Cu(3p) doublet is well fit with a FWHM of 3.2 eV. The binding energy of the Cu($3p_{3/2}$) photoelectron line is 75.1 eV, which corresponds to literature values for Cu_2O [15]. Next, determination of the FWHM of the Al(2p) component in Figure 4.1a was made by comparison of the Al(2p) photoelectron line for the single environment in bulk Al_2O_3 (FWHM = 1.9 eV). The Al(2p) binding energy value of 75.3 eV is characteristic of Al_2O_3 [16]. Metallic aluminum has a binding energy of 72.6 eV and was not observed [8]. Further information regarding the interface can be obtained from the Cu(L_3VV) Auger lineshape (Figure 4.1b). The Cu(L_3VV) Auger lineshape after 180 sec. of deposition (Figure 4.1b) displays a single oxidation environment. The Auger parameter value of 1846.3 eV is in the range of Auger parameters reported for other Cu(I) compounds [7]. The Cu(L_3VV) Auger lineshape is plotted as a function of a modified Auger parameter {α = KE of Cu(L_3VV) + BE of Cu(2p)} in order to correct for uniform charging effects [17,18]. With evidence of Al_2O_3 formation at the SiO_2 interface, grazing incidence Si(2p) spectra were

taken to monitor reduction of silicon. Si(2p) spectra at these low coverages proved to be insensitive to SiO_2 reduction. Grazing incidence spectra of the O(1s) photoelectron line (Figures 4.2a & 4.2b), however, proved to be more sensitive. A change in symmetry of the O(1s) photoelectron line (Figures 4.2a & 4.2b) accompanies deposition of the $Cu_{0.6}Al_{0.4}$ alloy. The FWHM of the O(1s) spectra for single environment SiO_2 (Figure 4.2a) was determined to be 2.5 eV. After 360 seconds of deposition, three environments

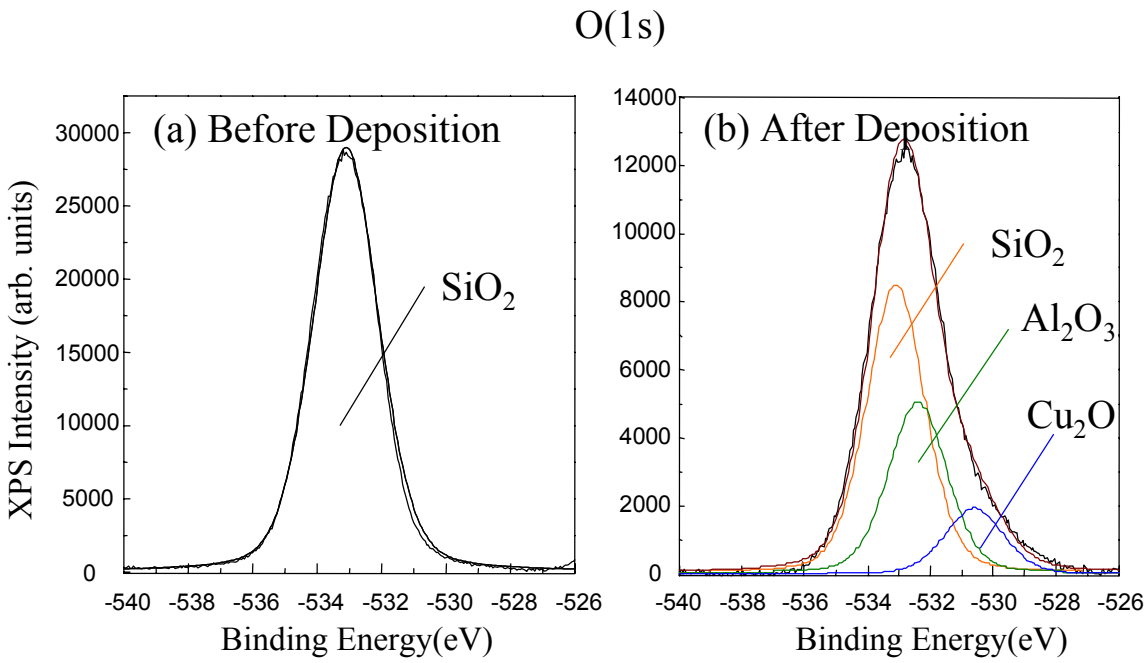

Figure 4.2. O(1s) Grazing Incidence XPS Spectra. (a) Before $Cu_{0.6}Al_{0.4}$ Deposition. (b) After 360 sec. of $Cu_{0.6}Al_{0.4}$ Deposition.

were employed to fit the O(1s) spectrum (Figure 4.2b). The binding energies at 533.1, 532.4, and 530.6 eV correspond to reported literature values for SiO_2, Al_2O_3, and Cu_2O [8,16; Haber, 1978 #82]. The Cu/Al atomic ratio was also calculated assuming the

stoichiometry of these fits and resulted in values within 5 % of the value calculated using the Al(2p) and Cu(3p) photoelectron lines.

4.3.2. Growth Modes

A $Cu_{0.6}Al_{0.4}$ film was sputter deposited onto SiO_2 in sequential depositions of 120 sec. each. After each deposition, the sample was transferred from the deposition chamber back to the main chamber for XPS analysis. The mode of growth of the $Cu_{0.6}Al_{0.4}$ film

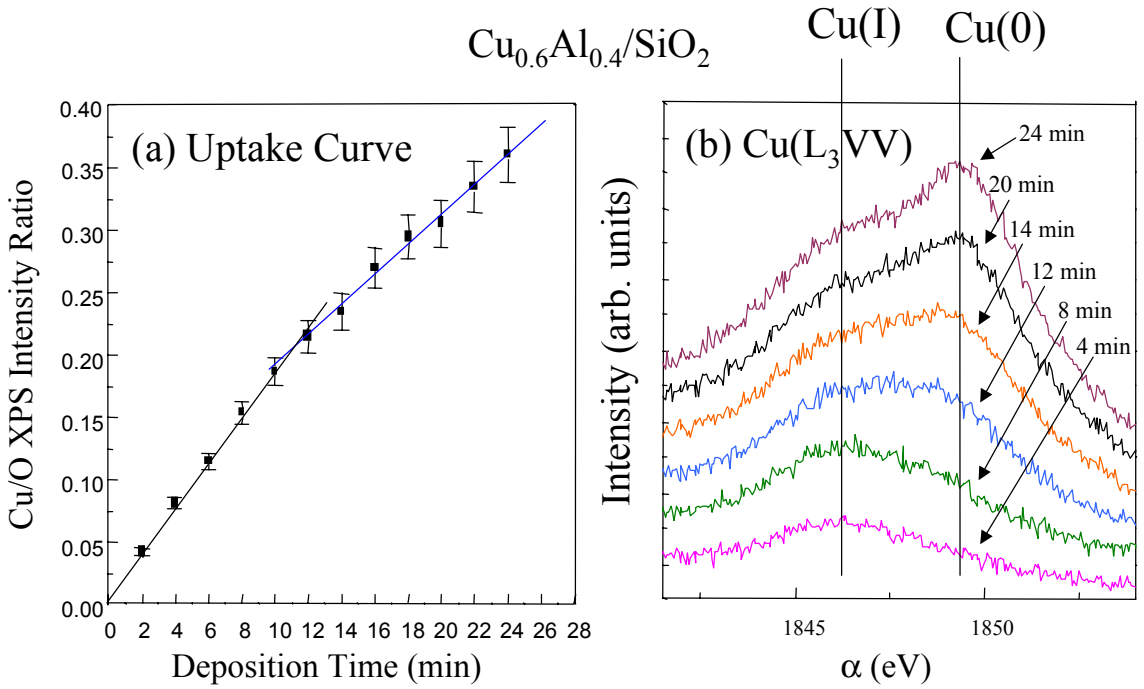

Figure 4.3. (a) $Cu_{0.6}Al_{0.4}/SiO_2$ Uptake Curve. (b) Cu(L_3VV) Evolution for $Cu_{0.6}Al_{0.4}/SiO_2$ as a Function of Deposition Time.

can be characterized by plotting the increase in copper or aluminum intensity relative to O(1s) intensity as a function of deposition time. The overlap of the Al(2p) and Cu(2p) region prohibits the derivation of an uptake curve based on aluminum coverage.

However, an uptake curve can still be derived using the intensity of the Cu($2p_{3/2}$) photoelectron line (Figure 4.3a). The change in slope of the uptake curve (Figure 4.3a) indicates conformal growth.[19, 20] Further information about the nature of the interface can be ascertained by observing the Cu(L_3VV) Auger lineshape as a function of deposition time (Figure 4.3b). The oxidation state of the Cu evolves with deposition time from Cu(I) to Cu(0). Cu(L_3VV) lineshape studies indicate that the feature at 1846.3 eV is associated with the presence of Cu(I), while the feature at 1849.3 eV is indicative of Cu(0) formation [21]. The Auger parameter of 1849.3 eV for is lower than that expected for bulk copper (1851.3 eV) [7]. This observation can be attributed to ineffective screening of Cu(0) at low coverages [19]. $Cu_{0.6}Al_{0.4}$ films deposited initially reacts with the surface to form Cu(I) species (Figure 4.3b) at the interface, *i.e.* copper "wets" the surface. At higher coverages, Cu(0) formation is observed (Figure 4.3b). Figures 4.3a and 4.3b indicate that formation of Cu(0) coincides with the change in slope in the uptake curve. The results in Figure 4.3a and 4.3b indicate that Cu initially deposited reacts to form a conformal ionic layer followed by formation of Cu(0). The surface coverage of Cu present at the break in the uptake curve is approximated as follows. First, we determine the fraction of oxygen intensity contributed by the first atomic layer:

$$\text{Fraction of Oxygen Intensity from First Atomic Layer} = \frac{\int_0^1 \exp(-x/\lambda)dx}{\int_0^\infty \exp(-x/\lambda)dx}, \qquad (4\text{–}2)$$

where λ is the mean free path in monolayers. A mean free path of 7.8 ML for the O(1s) photoelectron in SiO_2 is calculated using the equation derived by Powell *et al.*[20] Equation (4-2) yields the result that 12 % of the total oxygen intensity arises from the first atomic layer of the substrate. Next, the surface coverage of Cu in the first ad-layer is determined:

$$Cu / O = I_{Cu}A_O / 0.12 I_O A_{Cu} \qquad (4\text{-}3)$$

The copper surface coverage at the break in the uptake curve is approximately 0.31 ML (based on a Cu/O atomic ratio).

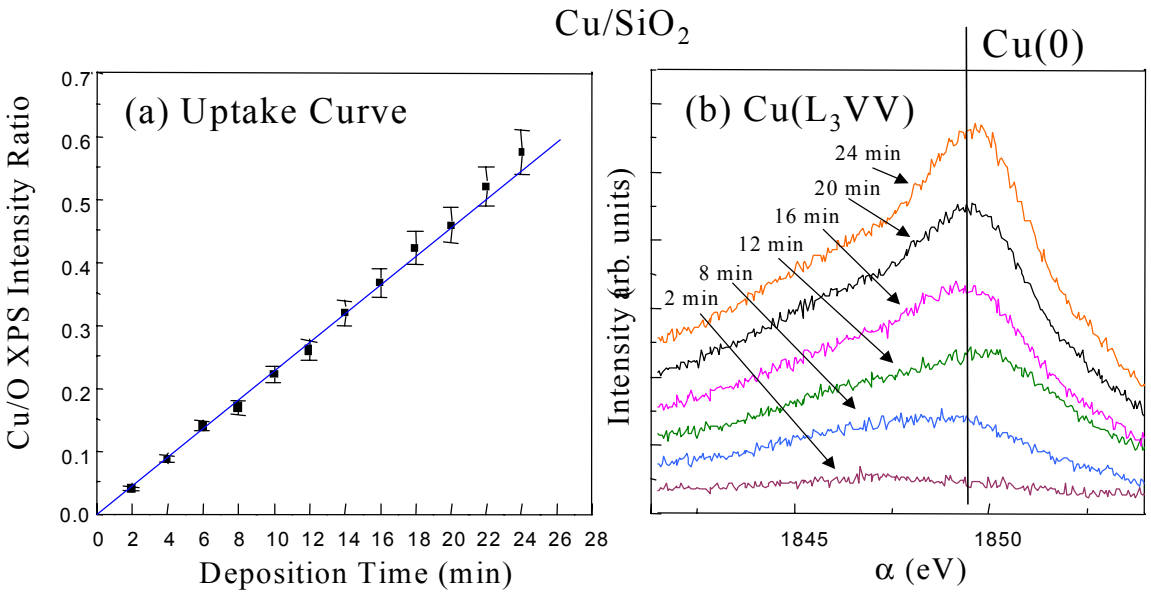

Figure 4.4. (a) Cu/SiO_2 Uptake Curve. (b) Cu(L_3VV) Evolution for Cu/SiO_2 as a Function of Deposition Time.

These data contrast with data obtained for Cu sputtered onto silicon oxide. Cu/O XPS intensity versus deposition time for Cu/SiO_2 results in linear behavior (Figure 4.4a). Futhermore, the feature at 1849.7 eV in the Cu(L_3VV) lineshape indicates formation of Cu(0) occurs at low coverages (Figure 4.4b) [21-23]. The Auger parameter value of 1849.7

eV is lower than that reported for bulk Cu which is 1851.3 eV [7]. The low value of the Auger parameter can be attributed to ineffective screening that occurs for metallic copper at low coverages [19]. The linear behavior observed is indicative of the formation of 3-dimensional nuclei, *i.e.* copper does not "wet" the surface.

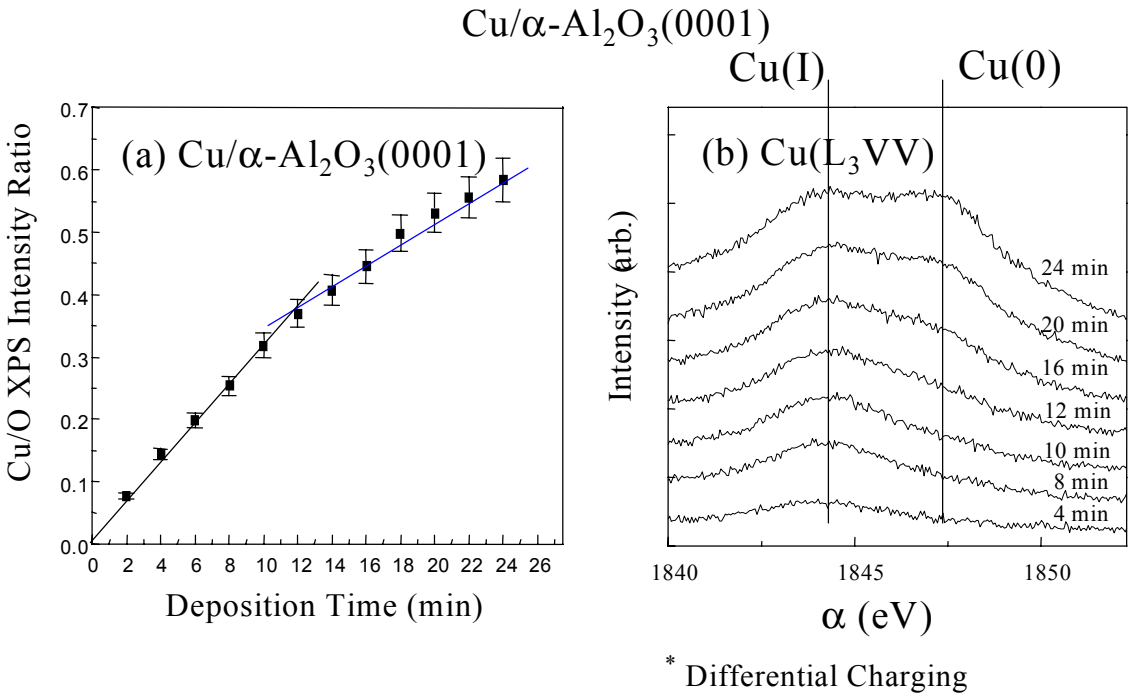

Figure 4.5. (a) Cu/α-Al_2O_3(0001) Uptake Curve. (b) Cu(L_3VV) Evolution for Cu/α-Al_2O_3(0001) as a Function of Deposition Time.

In order to compare the growth of $Cu_{0.6}Al_{0.4}/SiO_2$ and Cu/α-Al_2O_3(0001), Cu was sputtered onto sapphire at an operating pressure of 15 millitorr of Argon and 150 Watts. The mode of growth of copper sputter-deposited onto sapphire (Figure 4.5a) is similar to that observed for $Cu_{0.6}Al_{0.4}$ films deposited onto SiO_2 (Figure 4.4a). The change in slope of the uptake curve (Figure 4.5a) indicates conformal growth [24,25]. The Cu(L_3VV) Auger lineshape (x-ray excited), displayed in Figure 4.5b indicates that the oxidation state of Cu

evolves with deposition times. The shift in reported values in the Auger parameter, however, must be regarded with considerable skepticism due to differential charging of the sample. Differential charging is often observed on insulating samples and is more problematic than uniform charging [26,27]. Therefore, we rely on lineshape analysis [21-23] to characterize the electronic state of Cu rather than the values of the calculated Auger parameter. The data (Figure 4.5b) indicates Cu(I) formation for initial depositions of copper, *i.e.* copper "wets" the surface. At higher coverages, Cu(0) formation is observed. The appearance of Cu(0) in Figure 4.5b is coincident with the change in slope (Figure 4.5a). This indicates that initially deposited copper reacts with the surface to form a conformal ionic layer. Upon further depositions, Cu(0) formation is exclusively formed.

4.3.3. Thermal Stability of $Cu_{0.6}Al_{0.4}$ Films on SiO_2

$Cu_{0.6}Al_{0.4}/SiO_2$ and Cu/SiO_2 samples were annealed in UHV in 100 degree increments starting from 300 K. Following each anneal period (20min), the samples were cooled to room temperature and XPS spectra acquired. Annealing of Cu/SiO_2 resulted in a decrease of the Cu/O XPS intensity at 600 K (Figure 4.6a). Annealing of $Cu_{0.6}Al_{0.4}/SiO_2$ resulted in a decrease in the Cu/O XPS intensities only at 800 K and above (Figure 4.6b). Also, accompanying the decrease in Cu/O XPS intensity near 800 K is the change in lineshape of the x-ray excited Cu(L_3VV) Auger spectra (Figure 4.7). The change in lineshape (Figure 4.7) is marked by an increase in the intensity of Cu(0) relative to Cu(I). SEM images taken after annealing to 700 K (Figure 4.8a) indicates no evidence of dewetting. SEM images after annealing to temperatures greater than 800 K (Figure 4.8b), however, show Cu cluster formation and Cu "de-wetting" the surface. The

data therefore indicate that near 800 K, Cu de-wets from $Cu_{0.6}Al_{0.4}/SiO_2$ system and forms 3-D nuclei.

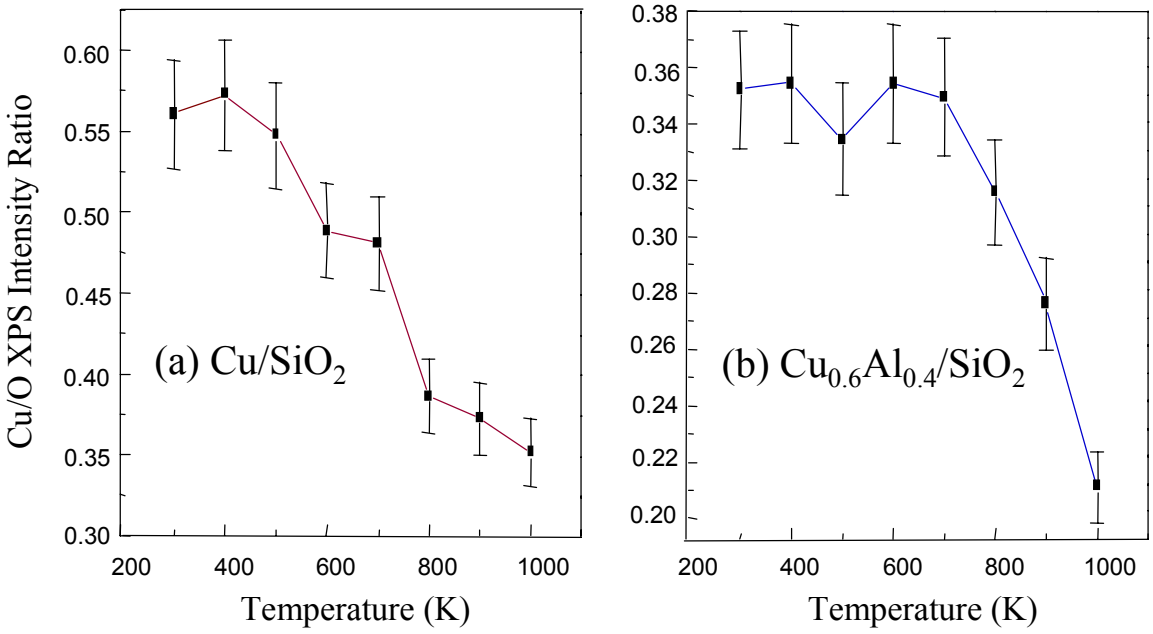

Figure 4.6. Cu/O XPS Ratio of (a) Cu/SiO_2 and (b) $Cu_{0.6}Al_{0.4}/SiO_2$ as a Function of Annealing Time.

4.4. Discussion

Uptake curves of Cu/SiO_2 (Figure 4.4a) exhibit no change in slope. This linear behavior demonstrates that copper does not "wet" SiO_2. In addition, Cu(L_3VV) spectra for Cu/SiO_2 (Figure 4.4b) indicate Cu(0) formation, further evidence of Cu-Cu interactions as would be expected in the formation of 3-D clusters. Our observation of the formation 3-D nuclei of Cu on SiO_2 is consistent with other reports in the literature [28]. Data for Cu/SiO_2 are in contrast to uptake curves for $Cu_{0.6}Al_{0.4}/SiO_2$ (Figure 3.3a). The uptake curves for $Cu_{0.6}Al_{0.4}/SiO_2$ (Figure 4.3a) along with the Cu(L_3VV) lineshape

evolution (Figure 4.3b) demonstrate that copper is deposited conformally when alloyed with aluminum. In addition to the uptake curve, the XPS spectra (Figure 4.1a & Figure 4.2) indicate that oxidation of Al and Cu has occurred after 360 sec of deposition. This is not surprising since the reduction of silicon oxide by aluminum is to be expected on the basis of the free energy formation of SiO_2 (192.4 kcal mol^{-1}) and Al_2O_3 (376.8 kcal mol^{-1}):[29]

$$3\ SiO_2 + 4\ Al \rightarrow 2\ Al_2O_3 + 3\ Si + 176.4\ kcal \qquad (4\text{-}4)$$

However, it is not clear in the case for $Cu_{0.6}Al_{0.4}/SiO_2$ if the oxidation of Al is solely a result of the reduction of SiO_2 or if the relatively high base pressure of the deposition chamber at 10^{-8} Torr contributes to the oxidation of Al at the SiO_2 interface on the time scale of the experiment. Irrespective of this uncertainty, it is clear that the oxidation of

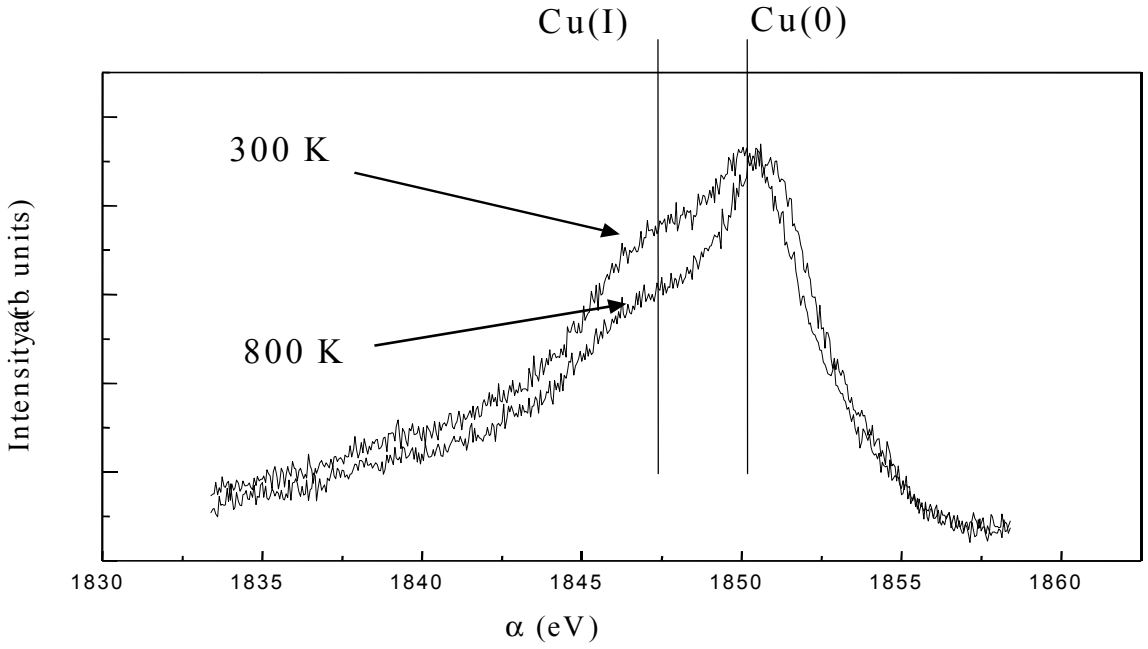

Figure 4.7. X-ray Excited Cu(L_3VV) Spectra of $Cu_{0.6}Al_{0.4}$ Films at 300 K and 800 K.

Al results in improved wetting of the copper at the SiO_2 interface. With the absence of metallic aluminum, we infer that aluminum segregates to the SiO_2 interface and forms Al_2O_3. Since Cu(0) formation is not observed for $Cu_{0.6}Al_{0.4}/SiO_2$ as in the case for Cu/SiO_2 in the first ad-layer, the data indicates that Cu is wetting a uniform interfacial alumina layer. Uptake curves for Cu/α-Al_2O_3(0001) (Figure 4.5a) show that Cu will wet α-Al_2O_3(0001). Furthermore, the x-ray excited Auger lineshape (Figure 4.5b)

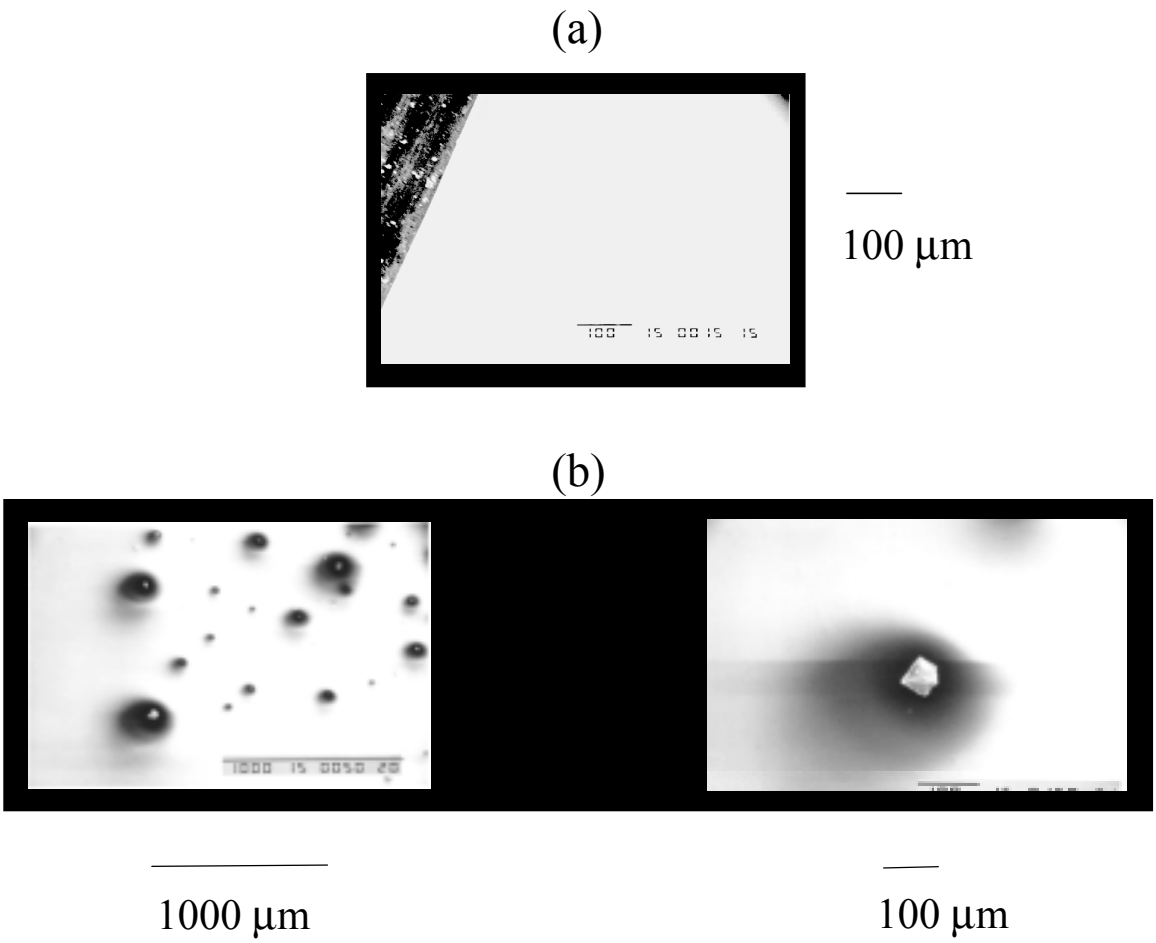

Figure 4.8. SEM Micrograph of $Cu_{0.6}Al_{0.4}/SiO_2$ annealed to (a) T ~ 700 K and (b) Dewetting observed for T > 800 K.

confirm only the presence of Cu(I) upon initial depositions, evidence of strong Cu-substrate interactions. These data (Figures 4.1-4.5) combine to indicate that Cu will not wet SiO_2, but will wet SiO_2 in the presence of Al. The data (Figures 4.1-4.5) suggest that the deposition of $Cu_{0.6}Al_{0.4}$ films results in formation of Al_2O_3 at the SiO_2 interface and results in formation of Cu(I) species in the first ad-layer.

Annealing studies performed on Cu/SiO_2 and $Cu_{0.6}Al_{0.4}/SiO_2$ (Figure 4.6) indicate a significant enhancement in the thermal stability of the $Cu_{0.6}Al_{0.4}$ films. Thermal stability is gauged by monitoring the Cu/O XPS intensity as a function of temperature. A decrease in the Cu/O XPS intensity can be attributed to copper 3-D cluster formation or copper diffusion into the substrate. Copper 3-D cluster formation results in attenuation of the Cu XPS intensity by other Cu atoms in the cluster. In addition, the formation of Cu clusters on the substrate surface results in less attenuation of the substrate signal and an increase in XPS substrate intensity. Cu/SiO_2, already a weakly interacting system at 300 K, exhibits a decrease in the Cu/O XPS intensity ~ 600 K (Figure 4.6). The decrease in Cu/O XPS intensity is consistent with the observed thermal diffusion of copper into SiO_2 for temperatures above 600 K [28]. $Cu_{0.6}Al_{0.4}/SiO_2$, in contrast, exhibits excellent thermal stability for temperatures up to 800 K (Figure 4.6). The presence of Cu(I) for temperatures up to 800 K (Figure 4.7) is evidence of strong Cu-substrate interactions. For temperatures above 800 K, SEM micrographs (Figure 4.8b) illustrate that de-wetting of Cu occurs in the $Cu_{0.6}Al_{0.4}/SiO_2$ system, rather than thermal diffusion.

The data combine to indicate that deposition of Cu onto SiO_2 at 300 K results in the formation of 3-D copper clusters. Annealing of these clusters at 600 K results in

thermal diffusion of copper into SiO_2. In contrast, $Cu_{0.6}Al_{0.4}$ films exhibit strong interactions between copper and the substrate up to 800 K. In addition, no evidence of thermal diffusion is observed for temperatures up to 800 K.

4.5. Conclusions

Sputter deposition from a CuAl (40 at. % Al) target onto SiO_2 resulted in the formation of a $Cu_{0.6}Al_{0.4}$ film. XPS spectra of the interface indicate that both Al and Cu have been oxidized in the first ad-layer. The results indicate that Al is present as Al_2O_3 at the SiO_2 interface. The data also indicate that formation of Al_2O_3 at the SiO_2 interface results in the ability of Cu to wet SiO_2. Uptake curves and Cu(L_3VV) spectra for Cu/α-Al_2O_3(0001) provide direct evidence that Cu wets Al_2O_3. Therefore, although Cu will not wet SiO_2, Cu will wet SiO_2 when alloyed with Al. In addition to the improved adhesion of Cu exhibited at the SiO_2 interface, the $Cu_{0.6}Al_{0.4}$ film displays excellent thermal stability for temperatures up to 800 K. The wetting interaction and thermal diffusion properties exhibited by the $Cu_{0.6}Al_{0.4}/SiO_2$ system is a significant improvement when contrasted with the Cu/SiO_2 system. Finally, the results here demonstrate the effectiveness of $Cu_{0.6}Al_{0.4}$ films as adhesion promoters and thermal diffusion barriers for Cu at the SiO_2 interface.

4.6. Chapter References

[1] Murarka, S. P. *Materials and Science Engineering* **1997**, *R19*, 85-151.

2] Murarka, S. P. *Metallization Theory and Practice for VLSI and ULSI*; Murarka, S. P., Ed.; Butterworth: New York, New York, 1992, pp Chap. 1.

[3] Mayer, J. W.; Lau, S. S. *Electronic Materials Science for Integrated Circuits in Si and GaAs*; Mayer, J. W.; Lau, S. S., Ed.; Macmiallan: Newy York, New York, 1990, pp Chap. 1.

[4] Ding, P. J.; Lanford, W. A.; Hymes, S.; Murarka, S. P. *J. Appl. Phys.* **1994**, *75*, 3627-3631.

[5] De Filipe, T. S.; Murarka, S. P.; Bedell, S.; Lanford, W. A. *Thin Solid Films* **1998**, *335*, 49-53.

[6] Shepherd, K.; Kelber, J. A. *Applied Surface Science* **1999**, *151*, 287-298.

[7] Moulder, J. F.; Stickle, W. F.; Sobol, P. E.; Bomben, K. D. *Handbook of X-ray Photoelectron Spectroscopy*; Moulder, J. F.; Stickle, W. F.; Sobol, P. E.; Bomben, K. D., Ed.; Physical Electronics, Inc.: Eden Prarie, Minnesota, 1992.

[8] Hollinger, G. *Appl. of Surf. Sci.* **1981**, *8*, 318.

[9] *ESCA Tools*; 4.6 ed.; Surface/Interface Inc., Mountain View, CA., 1995.

[10] Shirley, D. A. *Phys. Rev. B* **1972**, *5*, 4709.

[11] Sherwood, P. M. A. *J. Vac. Sci. Technol. A* **1995**, *14*, 1424.

[12] Wasa, K.; Hayakawa, S. *Handbook of Sputter Deposition Technology, Principles Technology and Applications*; Wasa, K.; Hayakawa, S., Ed.; Noyes Publications: Park Ridge, New Jersey, 1992, pp 304.

[13] Seah, M. P. *Practical Surface Analysis*; 2nd ed.; Seah, M. P., Ed.; John Wiley & Sons: New York, 1990; Vol. 1, pp 201-251.

[14] Lebugle, A.; Axelsson, U.; Nyholm, R.; Martensson, N. *Physica Scripta* **1981**, *23*, 825-827.

[15] Mcintyre, N. S.; Cook, M. G. *Anal. Chem* **1975**, *47*, 2208.

[16] Carley, A. F.; Roberts, M. W. *Proc. R. Soc. Lond. A.* **1978**, *63*, 403-424.

[17] Wagner, C. D.; Gale, L. H.; Raymond, R. H. *Anal. Chem.* **1979**, *151*, 466.

[18] Garenstroom, S. W.; Winograd, N. *J. Chem. Phys.* **1977**, *67*, 3500.

[19] Wu, Y.; Garfunkel, E.; Madey, T. E. *J. Vac. Sci. Technol. A* **1996**, *14*, 1662-1667.

[20] Powell, C. J.; Jablonski, A.; Tilinin, I. S.; Tanuma, S.; Penn, D. R. *Journal of Electron Spectroscopy and Related Phenoma* **1999**, *98-99*, 1-15.

[21] Shoen, G. *Journal of Electron Sprectroscopy and Related Phenomena* **1972**, *7*, 377.

[22] Fleish, T. H.; Mains, G. J. *Applications of Surface Science* **1982**, *10*, 51-62.

[23] Tobin, J. P.; Hirschwald, W.; Cunningham, J. *Applications of Surface Science* **1983**, *16*, 441-452.

[24] Somorjai, G. A. *Introduction to Surface Chemistry and Catalysis*; Somorjai, G. A., Ed.; John Wiley & Sons: New York, New York, 1994, pp 667.

[25] Feldman, L. C.; Mayer, J. W. *Fundamentals of Surface and Thin Film Analysis*; Feldman, L. C.; Mayer, J. W., Ed.; P T R Prentice-Hall, Inc.: EngleWood Cliffs, New Jersey, 1986, pp 352.

[26] Yu, X.-R.; Hantsche, H. *Surface and Interface Analysis* **1993**, *20*, 555-558.

[27] Barr, T. L. *J. Vac. Sci. Technol. A* **1989**, *7*, 1677-1683.

[28] Zhou, J. B.; Gustafsson, T.; Garfunkel, E. *Surface Science* **1997**, *372*, 21-27.

[29] Strausser, Y. E.; Scheibner, E. J.; Johannssen, J. S. *Thin Solid Films* **1978**, *52*, 203-214.

REFERENCES

ESCA Tools™; 4.6 ed.; Surface/Interface Inc., Mountain View, CA.: 1995.

An, C. H. and K. Sugimoto J. Electrochem. *Soc.* **1994**, *141*, 853-858.

Angyal, M. S., Y. Shacham-Diamand, et al. *Appl. Phys. Lett*. **1995**, *67*, 2152-2154.

Baba, K. and R. Hatada *Surface amd Coatings Technology* **1996**, *84*, 429-433.

Barr, T. L. *J. Vac. Sci. Technol. A* **1989**, *7*, 1677-1683.

Beamson, G. and D. Briggs *High Resolution XPS of Organic Polymers*: *The Scienta ESCA300 Database*; Beamson, G. and D. Briggs, Ed.; John Wiley & Sons: New York, New York, 1992; pp 26.

Broniatowski, A. *Phys. Rev. Lett*. **1989**, *62*, 3074.

Carley, A. F. and M. W. Roberts *Proc. R. Soc. Lond. A*. **1978**, *63*, 403-424.

Catania, P., J. A. Doyle, et al. *JVST* **1992**, *A 10*, 3318-3321.

Clevenger, L. A., N. A. Bojarczuk, et al. *J. Appl. Phys*. **1993**, *73*, 300-308.

Dalal, H. M., M. Ghafghaichi, et al. ; Dalal, H. M., M. Ghafghaichi, et al., Ed.; : U.S., 1980; Vol. 4 206 472.

De Filipe, T. S., S. P. Murarka, et al. *Thin Solid Films* **1998**, *335*, 49-53.

Diebold, U. *Physical Review B* **1993**, *47*, 3868-3876.

Ding, P. J., W. A. Lanford, et al. *J. Appl. Phys*. **1994**, *75*, 3627-3631.

Feldman, L. C. and J. W. Mayer *Fundamentals of Surface and Thin Film Analysis*; Feldman, L. C. and J. W. Mayer, Ed.; P T R Prentice-Hall, Inc.: EngleWood Cliffs, New Jersey, 1986; pp 352.

Fleish, T. H. and G. J. Mains *Applications of Surface Science* **1982**, *10*, 51-62.

Garenstroom, S. W. and N. Winograd *J. Chem. Phys*. **1977**, *67*, 3500.

Guinn, K. V., V. M. Donnelly, et al. *Surface Science* **1993**, *295*, 219-229.

Gupta, D. *Mater. Chem. Phys*. **1995**, *41*, 199-205.

Hollinger, G. *Appl. of Surf. Sci*. **1981**, *8*, 318.

Holloway, K., P. M. Fryer, et al. *J. Appl. Phys*. **1992**, *71*, 5433-5444.

Hung, L. S., F. W. Saris, et al. *J. Appl. Phys*. **1986**, *59*, 2416.

Jeng, S.-P., R. H. Havemann, et al. (1994). Process Integration and Manufacturability Issues for High Performance Multilevel Interconnect. Mat. Res. Soc. Symp. Proc., San Francisco, CA, MRS.

Jing-Cheng, L. and C. Lee *Electrochemical and Solid-State Letters* **1999**, *2*, 181-183.

Jirka, I. *Surf. Sci* **1990**, *232*, 307.

Kelber, J. A., C. Niu, et al. *Surface Science* **2000**, *446*, 76-88.

Kim, D. H., R. H. Wenterof Jr., et al. *J. Appl. Phys*. **1993**, *74*, 5164.

Klein, J. C., A. Proctor, et al. *Anal. Chem* **1983**, *55*, 2055.

Kolawa, E., J. S. Chen, et al. *J. Appl. Phys*. **1991**, *70*, 1369-1373.

Kolawa, E., P. J. Pokela, et al. *IEEE Electron Device Letters* **1991**, *12*, 321-323.

Kowalczky, S. P., R. A. Pollak, et al. *Phys. Rev. B* **1973**, *8*, 2387.

Larsson, K., C. Nordling, et al. *Acta. Chem. Scand*. **1966**, *20*, 2880.

Lebugle, A., U. Axelsson, et al. *Physica Scripta* **1981**, *23*, 825-827.

Li, J., Y. Shacham-Diamand, et al. *Mater. Sci. Rep*. **1992**, *9*, 1-51.

Loke, A. L. S., C. Ryu, et al. *IEE Electron Device Letters* **1996**, *17*, 549-551.

Mayer, J. W. and S. S. Lau *Electronic Materials Science for Integrated Circuits in Si and GaAs*; Mayer, J. W. and S. S. Lau, Ed.; Macmillan: New York, New York, 1990; pp Chap. 1.

Mcbrayer, J. D., R. M. Swanson, et al. *J. Electrochem. Soc*. **1986**, *123*, 1242.

Mcguire, G. E., G. K. Schweitzer, et al. *Inorg. Chem*. **1973**, *12*, 2451.

Mcintyre, N. S. and M. G. Cook *Anal. Chem* **1975**, *47*, 2208.

Miller, M. L. and R. W. Linton *Anal. Chem*. **1985**, *57*, 2314.

Moulder, J. F., W. F. Stickle, et al. *Handbook of X-ray Photoelectron Spectroscopy*; Moulder, J. F., W. F. Stickle, et al., Ed.; Physical Electronics, Inc.: Eden Prarie, Minnesota, 1992.

Murarka, S. P. *Metallization Theory and Practice for VLSI and ULSI*; Murarka, S. P., Ed.; Butterworth: New York, New York, 1992; Chap. 1.

Murarka, S. P. *Materials and Science Engineering* **1997**, *R19*, 85-151.

Murarka, S. P. and S. W. Hymes *Crit. Rev. In Sol. St. and Mat. Sci*. **1995**, *20*, 87-124.

Nicolet, M.-A. *Thin Solid Films* **1978**, *52*, 415-443.

Nicolet, M.-A. and M. Bartur *JVST* **1981**, *19*, 786-793.

Nicolet, M.-A., I. Suni, et al. *Solid State Technol*. **1983**, *26*, 129.

Nuesca, G. M. and J. A. Kelber *Thin Solid Films* **1995**, *262*, 224-233.

Pai, P. C. and C. H. Ting *IEEE Electron Device Lett*. **1989**, *10*, 423.

Peden, C. H. F., K. B. Kidd, et al. *J. Vac. Sci. Technol*. *A* **1991**, *9*, 1518-1523.

Powell, C. J., A. Jablonski, et al. *Journal of Electron Spectroscopy and Related Phenoma* **1999**, *98-99*, 1-15.

Prasad, J., G. Nuesca, et al. *Appl. Surf. Sci*. **1994**, *74*, 115.

Pretorius, R., J. M. Harris, et al. *Solid-State Electron* **1978**, *21*, 667.

Raghavan, G., C. Chiang, et al. *Thin Solid Films* **1995**, *262*, 168-176.

Reid, J. S., E. Kolowa, et al. *Thin Solid Films* **1993**, *236*, 319-324.

Sarma, D. D. and C. N. R. Rao *J. Electron Spectrosc. Relat. Phenom*. **1980**, *20*, 25.

Seah, M. P. *Practical Surface Analysis*; 2nd ed.; Seah, M. P., Ed.; John Wiley & Sons: New York, 1990; Vol. 1, pp201-251.

Shepherd, K. and J. A. Kelber *Applied Surface Science* **1999**, *151*, 287-298.

Sherwood, P. M. A. *J. Vac. Sci. Technol*. *A* **1995**, *14*, 1424.

Shirley, D. A. *Phys. Rev. B* **1972**, *5*, 4709.

Shoen, G. *Journal of Electron Sprectroscopy and Related Phenomena* **1972**, *7*, 377.

Singer, P. *Semiconductor International* **1999**, *13*, 67-70.

Somorjai, G. A. *Introduction to Surface Chemistry and Catalysis*; ed.; Somorjai, G. A., Ed.; John Wiley & Sons: New York, New York, 1994; pp 667.
Stampanoi, M., A. Vaterlans, et al. *J. Appl. Phys*. **1988**, *64*, 5321.

Stavrev, M., C. Wenzel, et al. *Applied Surface Science* **1995**, *91*, 257-262.

Strausser, Y. E., E. J. Scheibner, et al. *Thin Solid Films* **1978**, *52*, 203-214.

Tobin, J. P., W. Hirschwald, et al. *Applications of Surface Science* **1983**, *16*, 441-452.

Varma, S. and G. S. Chottiner *J. Vac. Sci. Technol*. *A* **1992**, *10*, 2857.

Venables, J. A., G. D. T. Spiller, et al. *Rep. Prog. Phys*. **1984**, *47*, 399.

Vijayakrishnan, V.; Rao, C. N. R. *Surface Science Letters* **1991**, *255*, L516-L522.

W. F. Egelhoff, J. *Surf. Sci. Rep*. **1987**, *6*, 253.

Wagner, C. D. *Discuss. Faraday Soc*. **1975**, *60*, 291.

Wagner, C. D., L. H. Gale, et al. *Anal. Chem*. **1979**, *151*, 466.

Wasa, K. and S. Hayakawa *Handbook of Sputter Deposition Technology, Principles Technology and Applications*; Wasa, K. and S. Hayakawa, Ed.; Noyes Publications: Park Ridge, New Jersey, 1992; pp 304.
Watts, J. F. *Vacuum* **1994**, *45*, 653-671.

Wiley, J. D., J. H. Perepezko, et al. *IEEE Transactions on Industrial Electronics* **1982**, *IE-29*, 154-157.

Wiley, J. D., J. H. Perpezko, et al. *IEEE Trans. Ind. Electron*. **1982**, *IE-29*, 154.

Wu, M.-C. and D. W. Goodman *J. Phys. Chem*. **1994**, *98*, 9874-9881.

Wu, Y., E. Garfunkel, et al. *J. Vac. Sci. Technol*. *A* **1996**, *14*, 1662-1667.

Yu, X.-R. and H. Hantsche *Surface and Interface Analysis* **1993**, *20*, 555-558.

Zhang, L., R. Persaud, et al. *Physical Review B* **1997**, *56*, 549-556.

Zhou, J. B., T. Gustafsson, et al. *Surface Science* **1997**, *372*, 21-27.

Zhou, J. B., H. C. Lu, et al. *Surface Science Letters* **1993**, *293*, L887-L892.

becomes oxidized. For copper coverages less than ~ 0.31 ML (based on a Cu/O atomic ratio), only Cu(I) formation is observed. At higher coverages, Cu(0) is observed. These data are in contrast with the observed behavior of copper metal deposited onto SiO_2 (Cu/SiO_2). The data for Cu/SiO_2 show that copper does not wet SiO_2 and forms 3-D nuclei. Furthermore, post-annealing experiments performed on $Cu_{0.6}Al_{0.4}/SiO_2$ show that neither de-wetting nor diffusion of copper occurs for temperatures up to 800 K, while Cu diffusion into SiO_2 occurs ~ 600 K. These data indicate that aluminum alloyed with copper at the SiO_2 interface serves as an effective adhesion promoter and thermal diffusion barrier.